Naval Research Laboratory

Washington, DC 20375-5320

NRL/MR/6950--00-8520

Channel-Constrained Process for Selective Electroless Metal Deposition

SUSAN L. BRANDOW
MU-SAN CHEN
WALTER J. DRESSICK

Laboratory for Molecularly Engineered Materials and Surfaces
Center for Bio/Molecular Science and Engineering

December 8, 2000

Approved for public release; distribution is unlimited.

20001220 164

REPORT DOCUMENTATION PAGE

Form Approved
OMB No. 0704-0188

Public reporting burden for this collection of information is estimated to average 1 hour per response, including the time for reviewing instructions, searching existing data sources, gathering and maintaining the data needed, and completing and reviewing the collection of information. Send comments regarding this burden estimate or any other aspect of this collection of information, including suggestions for reducing this burden, to Washington Headquarters Services, Directorate for Information Operations and Reports, 1215 Jefferson Davis Highway, Suite 1204, Arlington, VA 22202-4302, and to the Office of Management and Budget, Paperwork Reduction Project (0704-0188), Washington, DC 20503.

1. AGENCY USE ONLY (*Leave Blank*)

2. REPORT DATE

December 8, 2000

3. REPORT TYPE AND DATES COVERED

1 Jan. 1994 — 1 Oct. 2000

4. TITLE AND SUBTITLE

Channel-Constrained Process for Selective Electroless Metal Deposition

5. FUNDING NUMBERS

6. AUTHOR(S)

Susan L. Brandow, Mu-San Chen, and Walter J. Dressick

7. PERFORMING ORGANIZATION NAME(S) AND ADDRESS(ES)

Naval Research Laboratory
Washington, DC 20375-5320

8. PERFORMING ORGANIZATION REPORT NUMBER

NRL/MR/6950--00-8520

9. SPONSORING/MONITORING AGENCY NAME(S) AND ADDRESS(ES)

Shipley Co., Inc.
455 Forest Street
Marlborough, MA 01752

Office of Naval Research
800 North Quincy Street
Arlington, VA 22217-5660

10. SPONSORING/MONITORING AGENCY REPORT NUMBER

11. SUPPLEMENTARY NOTES

12a. DISTRIBUTION/AVAILABILITY STATEMENT

Approved for public release; distribution is unlimited.

12b. DISTRIBUTION CODE

13. ABSTRACT (*Maximum 200 words*)

Channel-constrained metallization (CCM) is described as a novel process for fabrication of metal features useful as etch-masks and electrical interconnects in microelectronics applications. The method creates a requisite surface reactivity template through patterned exposure and development of photoresist films to open channels to an underlying ligand self-assembled (SA) film. Subsequent electroless metal deposition occurs selectively at exposed ligand sites in the channels, which constrain lateral metal growth detrimental to feature critical dimension (CD) control during plating. A complete characterization of the individual process steps is presented; critical process issues include identification of appropriate photoresist/SA film combinations and exposure/development conditions that promote clearance of photoresist residues from the channels while maintaining adequate photoresist adhesion and feature CD control. The process has been demonstrated using both optical and e-beam exposure sources and is compatible with a wide range of substrates, including Si and planarizers, relevant for electronics applications. The high plasma etch selectivity of a thin Ni metal mask layer has been utilized in the fabrication of high aspect ratio structures ($\leq$5:1) in both Si and planarizer substrates with feature linewidths as small as ~100 nm.

14. SUBJECT TERMS

Electroless, Metallization, Additive, Microlithography, Monolayer, Semiconductor

15. NUMBER OF PAGES

34

16. PRICE CODE

17. SECURITY CLASSIFICATION OF REPORT	18. SECURITY CLASSIFICATION OF THIS PAGE	19. SECURITY CLASSIFICATION OF ABSTRACT	20. LIMITATION OF ABSTRACT
UNCLASSIFIED	UNCLASSIFIED	UNCLASSIFIED	UL

NSN 7540-01-280-5500

Standard Form 298 (Rev. 2-89)
Prescribed by ANSI Std Z39-18
298-102

CONTENTS

ABSTRACT....2

1. INTRODUCTION....2

2. EXPERIMENTAL SECTION....4

2.1 GENERAL MATERIALS....4

2.2 SELF-ASSEMBLED FILMS....4

2.3 PHOTORESIST FILMS AND IMAGING....5

2.4 METALLIZATION AND ETCHING....6

2.5 INSTRUMENTS....6

3. RESULTS AND DISCUSSION....7

3.1 PREPARATIVE STEPS....9

3.1.1 SELF-ASSEMBLED FILM SURFACE MODIFICATION....9

3.1.2 PHOTORESIST APPLICATION....11

3.2 LITHOGRAPHIC PERFORMANCE....13

3.2.1 FEATURE DENSITY DEPENDENT METALLIZATION....13

3.2.2 HIGH RESOLUTION FEATURES....18

3.2.3 ADHESION....22

3.2.4 PATTERN TRANSFER....24

4. SUMMARY AND CONCLUSIONS....28

5. ACKNOWLEDGMENTS....30

6. REFERENCES....30

Channel-Constrained Process for Selective Electroless Metal Deposition

Susan L. Brandow, Mu-San Chen, and Walter J. Dressick

Center for Bio/Molecular Science & Engineering (Code 6950)
Naval Research Laboratory
4555 Overlook Avenue, S.W.
Washington, DC 20375-5348

Abstract

Channel-constrained metallization (CCM) is described as a novel process for fabrication of metal features useful as etchmasks and electrical interconnects in microelectronics applications. The method creates a requisite surface reactivity template through patterned exposure and development of photoresist films to open channels to an underlying ligand self-assembled (SA) film. Subsequent electroless metal deposition occurs selectively at exposed ligand sites in the channels, which constrain lateral metal growth detrimental to feature critical dimension (CD) control during plating. A complete characterization of the individual process steps is presented; critical process issues include identification of appropriate photoresist/SA film combinations and exposure/development conditions that promote clearance of photoresist residues from the channels while maintaining adequate photoresist adhesion and feature CD control. The process has been successfully demonstrated using both optical and e-beam exposure sources and is compatible with a wide range of substrates, including Si and planarizers, relevant for electronics applications. The high plasma etching selectivity of a thin Ni metal masking layer has been utilized in the fabrication of high aspect ratio structures ($\leq$ 5:1) in both Si and planarizer substrates with feature linewidths as small as ~100 nm.

1. Introduction

The ability to fabricate spatially well defined, patterned, metal films on various substrates is critically important for numerous microelectronics applications. For example, fabrication of metal contacts and conductors is required in microwave circuits, printed wiring board (PWB) circuitry, local and global chip interconnects, and other aspects of electronics packaging technology [1]. Metal patterns are routinely used to define the opaque regions of reticles and masks for optical and x-ray lithography. Thin metal films have also been used as protective layers for pattern transfer in integrated circuit (IC) lithography, due to the extremely high etching resistance of metals and/or oxides derived from elements such as titanium [2], tungsten [3], zirconium [4], and nickel [5].

Many processes exist for metal pattern fabrication. Metal deposition techniques include sputtering, evaporation, chemical vapor deposition, electrolytic deposition, and electroless (EL) deposition. Of these, EL deposition [6] is particularly attractive in manufacturing because it offers the ability to metallize non-planar, insulating substrates with low temperature processes using simple materials and equipment at low cost. Approaches for producing lithographic patterns of metals are of two general classes: subtractive and additive. The traditional lift-off method is an example of a subtractive process, wherein metal is initially homogeneously deposited over an exposed and developed photoresist; the remaining resist must then be stripped to remove metal from the regions where it is

Manuscript approved November 16, 2000.

not required. Additive metallization is a simpler and less wasteful approach, and has distinct advantages in ease of processing and cost. A typical example of this approach involves initial deposition of a thin, homogeneous metal layer (by any of the above techniques) onto a substrate, followed by lithographic patterning of a resist to block selected regions of the underlying metal film. The exposed metal underlayer serves as either an electrode for electrolytic [7] up plating, or as a catalytic region for EL metal deposition [8]. However, even with these approaches the initial thin metal layer can lead to significant problems in the ultimate device structures, and subtractive steps must again be used to remove the buried metal. We therefore sought to develop an alternative process utilizing photolithography and molecular self assembly together to spatially control the binding of a Pd EL catalyst to a substrate and initiate EL metal deposition in a fully additive manner.

We have previously shown that self-assembled (SA) films of organosilanes containing ligand functional groups such as phosphines, pyridines, or alkylamines are useful for binding Pd catalysts to surfaces and that the bound catalysts initiate EL deposition [9-12]. These films are formed by chemisorption of alkoxysilane or chlorosilane precursors (typically of formula R_nSiX_{4-n}, where R contains the ligating group, X = Cl, OCH_3, or OC_2H_5, and n = 1-3) to hydroxyl groups on the surface of various substrates. Consequently, the R group is attached to the substrate surface via formation of covalent Si-O-substrate (siloxane) linkages [13, 14]. Treatment with Pd-based catalyst dispersions binds Pd to the ligand sites of the SA film, and subsequent immersion into an EL plating bath results in metal deposition on the catalyzed surface.

An important feature of this approach is that surface modification with organosilane SA films produces interfaces with well-defined, controllable chemical characteristics determined by the type and density of the surface functional groups [15, 16]. Subsequent chemical processes, such as selective catalyst binding and adherent EL metal deposition designed to occur at specific chemical surface sites, can then be performed on any substrate that can be modified with the appropriate SA film. We have shown [9-12] that a wide range of substrates [16], including silicon, ceramics, various metals and metal oxides, polymers (including fluoropolymers [17]), and diamond [18], can be metallized using this approach. This is a key concept for metal deposition in microelectronics because it can potentially eliminate the need to tailor the interfacial chemistry of metal deposition for the many different types of substrates required for particular applications.

EL metal patterns can be fabricated by several methods using ligating SA films. Direct exposure to radiation such as 193 nm laser light [9-11, 19, 20], extreme UV (EUV, 14 nm) radiation [19], focussed ion beams [19], or low voltage electrons from a scanning tunneling microscope [21, 22] (STM) induces chemical transformations in the SA film, creating a template of reactive functional groups on the surface. In one example of this process, the SA film intrinsically possesses ligating groups such as amines. Exposure to radiation impairs the ability of the amine to bind the Pd catalyst, and EL metallization occurs selectively in the masked regions of the surface. For high-resolution lithography, this approach is a true top surface imaging process, in which a latent image (and relief image [11] as well) is created in a SA film that can be as thin as ~0.5 nm. The EL metal selectively deposited onto the patterned SA film functions as an etching resistant masking layer that is highly effective for pattern transfer into the substrate. The process has successfully produced metal features with linewidths to ~20 nm using STM exposure [21].

We [23] and others [24] have investigated an alternative method for creating surface reactivity

templates that combines photoresist technology with organosilane SA film chemistry. In this approach, the requisite template of reactive surface functional groups is formed using a patterned photoresist or electron-beam resist to physically mask regions of a ligating SA film modified surface. Because Pd catalyst can bind only those ligands in the unblocked surface regions, EL deposition takes place selectively in channels created by the photoresist [25]. We provide here a detailed description of this channel-constrained metallization (CCM) process, characterization of its important process steps, and the results of lithographic processing studies that use the CCM process for fabricating patterned metal structures.

2. Experimental

2.1 General Materials- Deionized water of 18 MΩ resistivity was used for all experiments. All reagents were ACS reagent grade or better and were used as received unless otherwise noted. The organosilanes N-(2-aminoethyl)-3-aminopropyltrimethoxysilane (EDA), 2-(trimethoxysilyl)ethyl-2-pyridine (PYR), and 2-(diphenylphosphino)ethyltriethoxysilane (PHOS) from Hüls, Inc. were purified prior to use by vacuum distillation as follows: EDA (140°C, 14 mm Hg), PYR (105°C, 0.3 mm Hg) and PHOS (182°C, 1.3 mm Hg). Tridecafluoro-1,1,2,2-(tetrahydooctyl)-1-trichlorosilane (TDF) and m, p-(aminoethylaminomethyl)phenethyltrimethoxysilane (PEDA) from Gelest, Inc. were used without further purification. The organosilanes were stored under dry nitrogen atmosphere (from liquid nitrogen boiloff) until required for film preparations. Semiconductor grade NaOH (99.99%) and $Na_2PdCl_4 \cdot 3H_2O$ (99%) used for preparation of EL catalysts were both from Aldrich.

2.2 SA Films- p-type Si <100> wafers from Wafernet, Inc. and 1 in x 1 in fused silica slides (1 mm thick) from Dell Optics were cleaned using standard acid cleaning procedures as described elsewhere and stored in gently boiling water until needed for film formation [11]. To form an organosilane film, wafers and slides were removed from storage in boiling water, dried in a stream of filtered nitrogen gas (from liquid nitrogen boiloff), and immediately immersed in an organosilane treatment solution. Films of the PEDA silane were prepared by immersion in a solution containing methanol, water, and PEDA in the volume ratio 95:4:1 that was acidified with acetic acid to a concentration of ~10^{-3} M. After a deposition time of 20 min, the substrates were rinsed with methanol, dried, and baked on a hotplate at 120°C for 3 min. Films of EDA were also prepared according to this procedure, although a preferred batch processing method involved deposition from 1% (v/v) EDA in acidic aqueous solution, without the use of methanol. Alternatively, films of EDA were prepared by puddle coating spin rinsing as described later in the text. Films of PYR and PHOS were prepared by immersion in a 1% (v/v) solution of the organosilane in toluene that had previously been acidified with 10^{-3} M acetic acid. The solution was heated for 40 min to 65°C. The substrates were then rinsed twice in fresh toluene, then baked for 3 min at 120°C.

EDA, PEDA and PYR SA film thicknesses and homogeneity were determined by performing an 88-point scan with a Gaertner model 115C scanning ellipsometer using a procedure described elsewhere [26]. Optical constants for the clean Si substrates were determined immediately prior to film formation, giving values of 3.815 (± 0.076) for n_s and -0.153 (± 0.003) for k_s. The refractive indices used to calculate SA film thicknesses were 1.442 (EDA) [13], 1.5083 (PEDA) [13], and 1.46 (PYR) [27]. A refractive index value was not available for PHOS. Film thickness for this material was calculated from UV absorption measurements of the organosilane chemisorbed onto fused silica slides using a CARY 2400 UV-Vis Spectrophotometer as described elsewhere [28]. Film homogeneities

were determined by measurement of the sessile water drop contact angle at 6 points on treated Si wafers using a Zisman-type contact angle goniometer.

2.3 Photoresist Films and Imaging- AZPN (RAY-PN) electron beam photoresist was purchased from Hoechst, Inc. Thinner Type A and photoresists S1400, SNR-248, SNR-200.5 and SAL-601 were obtained from Shipley Co. S1400 photoresist was diluted from the as-received concentration of 27% solids with Thinner Type A to produce layers of varying thicknesses on SA film coated Si wafers: S1400-27 was spun at 4 krpm for 30 sec to produce films 1.3 μm thick; S1400-17 was spun at 4 krpm for 30 sec to produce 0.48 μm thick films; S1400-11 was spun at 5 krpm for 30 sec to produce 0.27 μm thick films. After spincoating, S1400 films were subjected to a post application bake (PAB) in a Grieve Model LW-201C oven (Grieve Corp.) at 90°C for 30 min. Planarizer films were fabricated by spincoating S1400-26 photoresist for 30 sec at 5 krpm or 6 krpm to produce 1.10 μm and 0.70 μm thick films, respectively, followed by thermal crosslinking at 210°C for 10 min using a Wentworth Labs Model TC-100 vacuum hotplate (Wentworth laboratories, Inc.). The resulting films were unaffected by rinsing with acetone and retained a sufficient concentration of surface hydroxyl sites to permit direct chemisorption of EDA organosilane. SNR-248 photoresist was spincoated at 4 krpm for 30 sec, then baked at 90°C (PAB) on the vacuum hot plate for 1 min to produce a film 0.96 μm thick. SNR-200.5 was spincoated at 4 krpm for 30 sec, then given a PAB at 105°C for 90 sec on the vacuum hotplate to produce a film 0.50 μm thick. SAL-601-ER2 films were spun at 4 krpm for 30 sec and baked in the oven at 75°C for 30 min to produce films ~0.2 μm thick for e-beam experiments. RAY-PN was spincoated for 30 sec at 5 krpm and then subjected to a PAB at 100°C for 2 min on the vacuum hotplate to form a 0.30 μm thick film. SAL-601-ER7 was diluted 1:3 (v/v) with Shipley Thinner Type A, spincoated at 5 krpm for 30 sec, and subjected to a PAB at 75°C for 30 min on the vacuum hotplate to produce films of ~68 nm thickness on the EDA coated S1400 planarizer for EUV experiments. All photoresist film thicknesses were determined using a Tencor Alpha-Step 500 Surface Profilometer.

Optical exposure tools included a Karl Suss standard UV (365-405 nm output) Hg lamp contact aligner, a Suss MJB3 deep UV (220-230 nm) Hg lamp contact aligner, and a GCA 0.35 NA XLS 200 Laserstep 5x reduction KrF laser-based (248 nm) projection stepper. Exposure doses with the lamp based exposure source was calculated by multiplying the measured power output at 254 nm (deep UV; typically 4-5 mW/cm^2 at the wafer plane) or 365-405 nm (standard UV; typically 10 mW/cm^2 at the wafer plane) by the exposure time. For EUV lithography, exposures were made at 13.4 nm using a first generation 10x Schwarzchild camera with a nominal field size of 0.4 mm diameter. For e-beam lithography a JEOL 50 keV e-beam Nanowriter was used as the exposure tool. For each exposure tool, a range of doses consistent with the photoresist was investigated: Karl Suss standard UV (365-405 nm output) Hg lamp contact aligner with S1400 (20-200 mJ/cm^2); Suss MJB3 deep UV (220-230 nm) Hg lamp contact aligner with SAL-601-ER7 (5-10 mJ/cm^2) or S1400 (10-50 mJ/cm^2); GCA 0.35 NA XLS 200 Laserstep 5x reduction KrF laser-based (248 nm) projection stepper with SNR-248 or SNR-200.5 (5-60 mJ/cm^2); 13.5 nm EUV Schwarzchild camera and SAL-601-ER7 (1-25 mJ/cm^2); JEOL 50 keV e-beam Nanowriter and SAL-601-ER2 or RAY-PN (10-50 μC/cm^2). Following exposure, all photoresist films (except S1400) were subjected to a post-exposure bake (PEB) using the vacuum hotplate: specific PEB conditions for each photoresist are given later in the text and figure captions.

The developers CD-14, MF-312, MF-319, and XP89-114 were all from Shipley Company.

MF-312 concentrate contains tetramethylammonium hydroxide (TMAH) at a concentration of 0.54 M and is usually diluted 1:1 to make the working developer solution. Alternatively, MF-312 (CD-27) developer from Shipley was used, which is supplied at the diluted TMAH concentration of 0.27 M. For the EUV experiments, a 0.24 M MF-312 developer solution was prepared by dilution of the MF-312 concentrate. Development times and conditions, together with exposure doses, were varied as described in the text to achieve optimal clearing of photoresist channels for metallization; specific protocols corresponding to the best conditions for selective metal deposition are cited in the text and figure captions.

2.4 Metallization and Etching- The preparation of the **PD1** catalyst has been described elsewhere [29]. **PD2** catalyst was prepared as described in the literature [30] with the following single change in procedure: following addition of the 82 mM aliquot of HCl (aq) solution to arrest development of the colloid, the dispersion was diluted 1:1 (v/v), rather than 3:1 (v/v), with 1.0 M NaCl (aq) solution to complete the catalyst preparation. Contact times of the dispersions with the SA film surfaces are typically 20-30 min for **PD1** and 2-3 min for **PD2**. For PHOS SA films, however, contact times were increased to 30-60 min for **PD1** and 5-10 min for **PD2** to obtain suitable plating.

Electroless metallization of catalyzed substrates was by immersion into a NIPOSIT® 468 (Shipley Co.) nickel-boron plating bath. The bath was prepared as required by mixing the "M", "B" and "A" component solutions and adjusting the solution pH to 7 as directed by the manufacturer. For most experiments, we diluted the bath with DI water to 10% of the original strength and readjusted to pH 7.0 with H_2SO_4. Plating times of ~5-30 min at a bath temperature of 25°C were typically used, giving an estimated thickness of the Ni deposit of ~10-50 nm. For certain experiments, however, the full strength bath was used at elevated temperatures (50 ± 3°C) for metallizations. Baths were also prepared in which individual components (*i.e.*, "M", "B", or "A") were varied through a range of 50-200% of their usual values to evaluate the influence of bath composition on feature plating. Specific experiments utilizing these modified baths are described later in the text.

After metallization, unexposed S1400 films were stripped by spraying the wafer with a stream of acetone for ~10 sec, followed by rinsing with DI water and drying under nitrogen. SNR-248 and SAL-601 films were stripped using Shipley XP-91140 Remover at 85°C for 10-60 sec. RAY-PN films were likewise stripped with Shipley XP-91140 Remover for 10 sec at 80°C. SNR200.5 films were removed by SO_2-O_2 plasma etching using a Vortex Model 5410 helicon source etcher (Lucas-Signatone, Inc.) [31]; a mixture of 4 sccm SO_2 and 1 sccm O_2 at 2 mTorr and 2.5 kW RF power with 100 W sample chuck bias power gave an etching rate of ~0.81 μm/min.

Metal patterns on Si wafers were transferred into the Si substrate by reactive ion etching (RIE) in SF_6-CHF_3 plasmas using a Plasmatherm 500 Series etcher. Using a mixture of 4 sccm SF_6 and 3 sccm CHF_3 at 20 mTorr and 100 W RF power gave an etching rate of ~15 nm/min. Metal patterns on the S1400 planarizer film were transferred through the planarizer to the Si wafer surface using the Plasmatherm 500 etcher with an O_2 plasma; a 10 mTorr O_2 plasma at 55 W RF power gave an etching rate of 45 nm/min. Wafers were held on a water-cooled chuck (22 ± 1°C) during etching. Ni metal films were removed following etching by rinsing the wafer with dilute HNO_3 (aq) solution.

2.5 Instruments- Atomic Force Microscope (AFM) images were collected on a commercial Nanoscope III instrument (Digital Instruments) equipped with microfabricated cantilevers using the

Tapping Mode or Error Signal Mode. AFM tips were treated by immersion in TDF organosilane to minimize adhesion of the tip to photoresist surfaces during scanning. Data processing consisted of a correction to account for sample tilt followed by application of a median filter. Substrate images were obtained at various stages of the CCM process using a Cambridge Leica FE360 scanning electron microscope (SEM) or a Nikon AFX-IIA optical microscope. Auger linescans were collected using a PHI 660 Auger Electron Spectrometer (AES). X-ray photoelectron spectroscopy (XPS) and Rutherford Backscattering Spectrometry (RBS) were performed as described previously [11].

3. Results and Discussion

Channel-constrained metallization (CCM) is a bi-level, multi-step, lithography process; the steps comprising the process are illustrated in Figure 1. First, the surface of the substrate to be metallized is modified by chemisorption of a ligating organosilane SA film at surface hydroxyl sites on the substrate. For materials such as poly(hexafluoropropylene-*co*-tetrafluoroethylene (*i.e.*, FEP) [17], diamond [18], or polymer planarizers, whose surfaces possess few, if any, hydroxyl sites, an oxygen plasma etch (step not shown) must be performed to generate the requisite OH sites prior to silane chemisorption. The ligand group of the organosilane is chosen such that it exhibits a high affinity for covalent binding to Pd(II). Appropriate ligands include alkylamines, pyridines and phosphines, among others [32]. The structures and abbreviations of the ligand silanes used in this study, together with their sessile water drop contact angles and solution pK_a's, are shown in Figure 2 (next page).

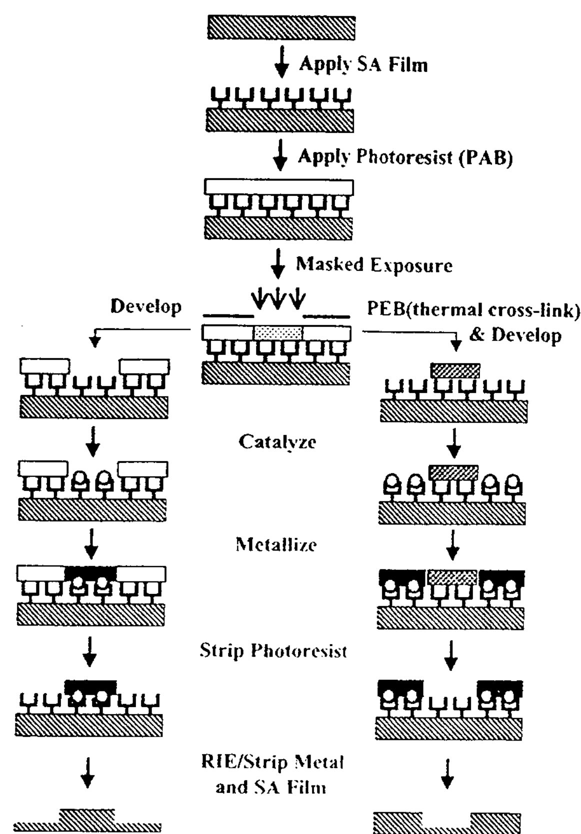

Figure 1. Channel-Constrained Metallization Process Steps. Positive tone photoresist processing (left branch) and negative tone photoresist processing (right branch) sequences are shown. Goalpost structures represent metal ligand sites.

In the next step, a photoresist is applied to the modified surface using standard spincoating procedures. This step includes a post application bake (PAB, not shown) to drive excess solvent from and adhere the photoresist to the underlying SA film. Subsequent exposure using an appropriate radiation source through a patterned mask creates an image of the mask in the photoresist. The image is defined by the chemical changes induced in the photoresist during irradiation. Irradiation leads to chemical changes that promote (positive tone) or hinder (negative tone) solubility of the photoresist film during the subsequent development step. For example, positive tone photoresists typically utilize mixtures of mono-, bis-, and tris-cresol esters of 2-diazo-1-naphthoquinone-5-sulfonic acid (DNQ) as the photoactive compounds (PAC) in the resist formulation [33]. Although these materials are nearly insoluble in basic aqueous solution, irradiation converts the DNQ to the corresponding indene

carboxylic acid via a Wolf rearrangement. The formation of the carboxylate during subsequent pattern development with an aqueous base solution solubilizes the irradiated regions of the photoresist, creating a channel uncovering the underlying ligand SA film.

In contrast, negative tone photoresists rely upon polymer crosslinking reactions to greatly decrease the solubility of the irradiated areas of the photoresist. In general, these are comprised of low molecular weight phenolic (*e.g.*, polyvinylphenol or novolak) resins, an acid-activated crosslinking agent, and a photoacid generator (PAG). The chemistry underlying this class of photoresists is illustrated in eqs 1-3 (note Scheme 1) using hexamethoxymethylmelamine (MEL) as a crosslinking agent and 2,6-dinitrobenzyltosylate (DNBT) as a PAG [34]. Photoresist irradiation releases toluenesulfonic acid into the film through the photodecomposition of DNBT to 2-nitroso-6-nitrobenzaldehyde according to eq 1. During a post exposure bake (PEB), MEL is attacked by the acid and converted into a strong alkylating agent in eq 2 through loss of methanol. Alkylation of the novolak in eq 3 initiates the crosslinking, releasing additional acid to propagate the reaction. The solubility of the highly crosslinked material formed in the irradiated areas of the photoresist is sufficiently low to allow pattern development to proceed. For a given exposure mask, note that the areas of SA film uncovered during development of the negative tone photoresist are complementary to those uncovered using a positive tone photoresist. That is, a pattern of ligand reactivity and, consequently, deposited metal of opposite tone is obtained using the negative tone photoresist.

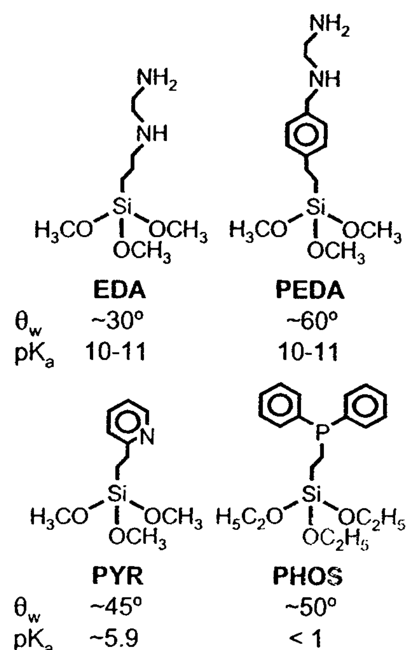

Figure 2. Structures and Properties of the Organosilane Film Precursor Molecules

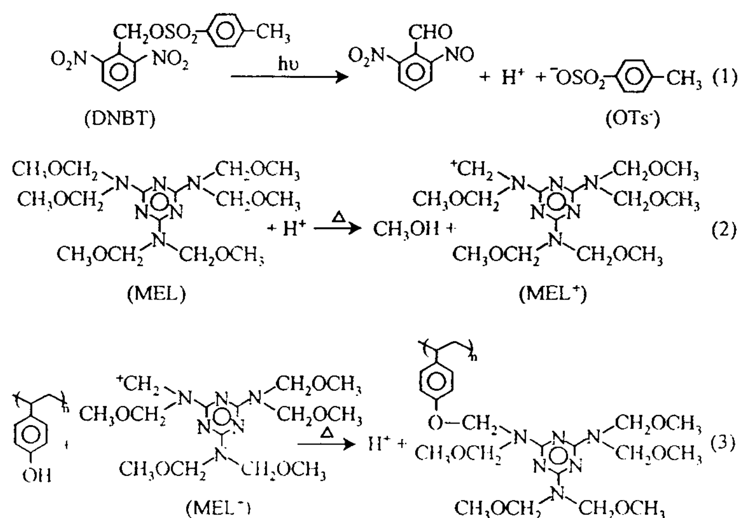

Scheme 1. Example of negative-tone chemically amplified photoresist crosslinking chemistry

Following development, treatment with the catalyst solution binds Pd(II) only to the unmasked ligand sites and not to the surface of the photoresist. Immersion of the selectively catalyzed substrate in an EL metal deposition bath reduces the bound Pd(II) to Pd metal, which initiates autocatalytic deposition of the EL metal in the pattern channels. As metal deposition continues, the channel walls constrain lateral metal growth that might otherwise distort the original image. Metallization is terminated following the deposition of a ~20-30 nm thick

metal film and the remaining photoresist is chemically stripped from the substrate. The patterned metal film remaining is of opposite tone from the mask image whenever a positive tone photoresist is used in the CCM process and identical in tone to the mask image if a negative tone photoresist is used. In the final steps, the metallized substrate is subjected to a reactive ion etch (RIE) in a plasma chamber. Because areas covered by the metal film are highly resistant to degradation during etching compared to the uncovered regions of the substrate, selective etching of the pattern is promoted. Following completion of the RIE, the metal pattern is removed by dissolution in acid solution. In this manner, transfer of the original photoresist image into the underlying substrate is completed.

The steps comprising the CCM process can be classified as either lithographic or preparative steps. Lithographic steps are those procedures that directly involve creation of an image and transfer of that image into the substrate. Image creation steps are those processes leading to formation of the pattern on the substrate. These include masked irradiation and development of the photoresist as well as the selective deposition of metal in the photoresist channels. Pattern transfer into the substrate occurs solely through the RIE step.

Preparative steps are those processes primarily related to the general preparation of the substrate. In Figure 1, these include the application steps for both the SA film and photoresist and the removal of both photoresist following metallization and metal after the RIE. Although these processes are independent from the lithographic steps, they do determine properties of the SA film and photoresist layer and therefore can affect lithographic performance. For example, the SA films used must possess sufficient resistance to base hydrolysis to maintain adequate surface ligand densities following photoresist development to initiate and sustain EL metal deposition. Furthermore, because photoresists absorb light strongly at higher energies, thinner resists are required to ensure that imaging occurs through the entire thickness of the resist film. Photoresist-substrate interactions must therefore be optimized to provide a uniform film for imaging free from pinhole defect sites capable of supporting spurious metal growth. Consequently, it is critically important to characterize and understand the preparative steps to successfully implement the CCM process.

In this report, we first discuss and characterize the chemistries underlying the preparative steps of the CCM process. These include various aspects of SA film formation and reactivity, control of pinhole density in thin photoresist films and general aspects of metallization selectivity. We next evaluate photoresist exposure and development, patterned metal deposition, and RIE process steps comprising the lithographic steps. In each case, the evaluation process emphasizes the identification and control of factors affecting lithographic performance.

3.1 Preparative Steps

3.1.1 SA Film Surface Modification- The SA film surface modification step can be viewed as analogous to the process of vapor priming Si wafers with hexamethyldisilazane to enhance photoresist adhesion in standard processing operations; however, in this case the modified surface possesses metal binding sites rather than terminal methyl groups. Formation of organosilane films with ligating functional groups is generally performed by dipcoating from non-polar (such as toluene or hexane) or aqueous alcoholic solutions [13, 14] as described in the Experimental section. Due to the solubility of alkylamine silanes such as EDA in water, films of these materials can also be produced by dipcoating from a wholly aqueous solution, thus eliminating the need for organic solvents. However, for ultimate

use of the CCM approach in a manufacturing environment, it is preferable to adapt the SA film formation process to be compatible with standard wafer track system processing. We therefore first performed a study to determine the thickness, homogeneity, functional group surface density, and metallization coverage for SA films deposited using a spincoating apparatus.

Aqueous solutions of EDA (1% or 5% organosilane by volume) containing 1 mM acetic acid as a film deposition catalyst were applied as a puddle onto a Si wafer that was held by vacuum onto the chuck of a spinner. After deposition times of 1 min or 2 min, the wafer was spun at 3 krpm for 15 sec under a stream of DI water, and then spun dry for an additional 15 sec. The coated wafers were baked to complete the dehydration reaction that forms the siloxane bond between the organosilane and the substrate.

Coating thickness and homogeneity were evaluated by ellipsometry. All combinations of EDA concentration and deposition time yielded film thicknesses that ranged between 4 Å and 6 Å, which are typical of a dipcoated EDA film [35]. The 3σ variation in thickness was found to be < 2 Å, indicative of excellent film uniformity across the wafer. The density of amine functional groups on the wafer surface was determined from the ratio of the nitrogen to silicon peaks obtained using XPS. N/Si ratios of 7.7% to 8.1% were found for the various deposition conditions employed. These values are not significantly different given the accuracy of the measurement technique, and compare favorably to the typical N/Si ratios of 7 to 8% routinely obtained by us for dipcoated films. Subsequent treatment of the EDA coated wafers prepared by the puddle deposit/spin rinse method with either **PD1** or **PD2** EL catalyst followed by immersion in an EL Ni bath at room temperature for 30 min initiated Ni deposition. The metal plated homogeneously across the entire wafer and the metal adhesion was sufficient to pass a tape peel test. Consequently, these experiments indicate that the puddle coat/spin rinse approach can be used to reproducibly fabricate EDA films on Si substrates that are identical in thickness, homogeneity, density of amine groups, and reactivity towards EL metal deposition to those produced by the dipcoated SA films [10].

An additional and key area of concern with the CCM process is the stability of the SA film layer during the photoresist development step. The presence of sufficient surface ligand density to initiate EL metal deposition in those areas of the SA film uncovered following photoresist development is a critical requirement for the CCM process. Because siloxane bonds are susceptible to nucleophilic attack by hydroxide ion (such as is present in aqueous base photoresist developers), removal of the organosilane film from the substrate will eventually occur in the presence of base. We therefore set out to quantify the extent to which exposure to MF-312, a TMAH-based developer, affects the density of amine groups of the EDA silane film and also how this affects the ability of the EDA surface to be metallized.

Si native oxide substrates were modified with EDA films, treated with MF-312 (CD-27) developer for times ranging up to 8 minutes, and then rinsed with DI water. The longer times were chosen to approximate the longest possible time that the EDA film surface would be exposed to the developer during CCM processing. XPS results showed a monotonic decrease of the surface N/Si ratio from the characteristic initial value of 7.5% to ~6.7% after 2 min, ~6.2% after 4 min and ~5.1% after 8 min in MF-312. However, all samples metallized homogeneously. These results clearly show that the expected attack of OH^- at the organosilane film occurs, with the resulting removal/destruction of some of the amine functionality from the surface. An analogous result has also been observed

upon exposure of another ligating SA film, prepared from 2-pyridylethyltrimethoxysilane (PYR), to an aqueous solution of NaOH at a similar concentration to the MF-312.

EDA surfaces exposed to MF-312 for varying times were treated with **PD2** EL catalyst for 2 min and then plated with the 10% NIPOSIT® 468 bath for 30 min. All samples plated homogeneously. Therefore, although base hydrolysis of the organosilane film can be a concern at extended development times, it apparently does not adversely affect metallization in the CCM process for development times $\leq$8 min.

3.1.2 Photoresist Application- In the second step of the CCM process (Figure 1), a commercial photo- or electron-beam resist is spincoated onto the SA film-modified substrate surface. The primary concerns associated with this step include (i) maintenance of adequate photoresist adhesion to the substrate, (ii) control of photoresist uniformity (especially with respect to pinhole formation for thinner films), and (iii) the assessment of the general ability of the photoresist to itself resist metallization. Photoresist adhesion issues are intimately associated with exposure and development processes and will be discussed in section 3.2.3 below. We address here issues of photoresist film defects and general resistance towards metallization.

For IC lithography, photoresist thicknesses of approximately 1 μm are required to provide the necessary etching resistance in traditional single level processes. However, as optical exposure tools shift to shorter wavelength sources and higher numerical aperture lenses to improve resolution, resist opacity increases and the depth of focus (DOF) budget may not be adequate to print a focussed image in the micron-thick layer.[1] However, in the CCM process, the selectively deposited metal serves as the etching resistant component so the photoresist need only function as the imaging layer to create the channel for metallization. The photoresist thickness can therefore be adjusted in the CCM process to meet the transparency and DOF requirements of various exposure systems. For example, UV spectroscopy of S1400 photoresist on fused silica substrates gives values ~0.33 a.u./μm at 436 nm, ~0.65 a.u./μm at 365 nm, ~2.12 a.u./μm at 254 nm, and ~23.4 a.u./μm at 193 nm. Transparency is clearly adequate at 436 nm and 365 nm, but not at 254 nm and 193 nm, to expose the entire thickness of a 1 μm thick film. Proper transparency can be achieved at the latter wavelengths only through the use of thinner films. For example, 193 nm light will be completely attenuated (*i.e.*, film absorbance $\geq$ 2) by S1400 films of thickness $\geq$ 85 nm; significantly thinner films would therefore be required for use in the CCM process.

Unfortunately, the tendency to the form pinholes and related defects increases as film thickness is decreased. Consequently, the production of very thin films with sufficiently low defect densities for manufacturing constitutes an issue generic to bilevel imaging schemes with severely attenuated radiation (*e.g.*, 13 nm EUV). An advantage of the CCM process in this regard is that it is only defects in the hard mask, rather than the photoresist, that ultimately matter: any

---

[1] The depth of focus (DOF) for a projected image can be estimated using the equation: $DOF = k\lambda/(NA)^2$, where k is a constant that is characteristic of the process, λ is the wavelength of the exposure source, and NA is the numerical aperture of the optical projection lens [36]. For i-line (365 nm) Hg lamp exposure and k = 0.7, DOFs for exposure tools with various NA lenses are: 1.24 μm (0.45 NA), 0.83 μm (0.55 NA), and 0.60 μm (0.65 NA). The same calculation using k = 0.6 yields: DOF = 1.06 μm, 0.70 μm and 0.50 μm, respectively, for the three NA values. Therefore, the use of higher NA exposure tools to achieve improved resolution may not be possible with a single level resist approach due to DOF limitations.

pinholes in the photoresist that do not promote metal deposition are irrelevant. We therefore investigated the dependence of pinhole density on photoresist film thickness using EL metal deposition to identify defects that could compromise the CCM process. SAL-601 photoresist exposed using EUV (13 nm) radiation was chosen as a model system. Negative tone photoresists such as SAL-601 were preferred for high energy exposures because they exhibited superior abilities to control post-development residues compared to S1400 and related positive tone systems (*vide infra*). Furthermore, for 13 nm exposures it had been previously determined that optimal feature printing required SAL-601 films of only ~65-70 nm thickness using a single level lithography process [37]. SAL-601 photoresist exposed at 13 nm was therefore ideally suited to determine whether photoresist films free from metallizable defects could be fabricated at thicknesses appropriate for high energy exposures using our process.

SAL-601 films were spincoated onto substrates using different photoresist dilutions and spin speeds to vary the thickness of the film. Studies were carried out on EDA-coated Si wafers and a planarizer comprised of thermally crosslinked S1400 photoresist likewise coated with EDA. The minimum SAL-601 film thickness obtained in each case, as determined by profilometry, was ~60 nm. Following deep UV flood exposure (5 mJ/cm^2) and PEB (115°C, 1 min), samples were developed with MF312 (70 sec), catalyzed with **PD1** (30 min) and immersed in 10% strength, room-temperature NIPOSIT® 468 EL Ni bath for 10 min. Following metallization, a circular area of diameter 4.5 cm at the center of each substrate was examined using an optical microscope (400x) to tabulate the number of metal point defects. For the Si wafer, 16 defects were noted for a 100 nm thick film. Decreasing the film thickness to 70 nm increased the number of defects to 19. In contrast, for SAL-601 films spincast onto the S1400 planarizer, no defects were observed for films $\geq$ 65 nm in thickness. The origin of the different behavior noted for each substrate is uncertain; it may simply reflect, at least in part, differences in film adhesion or quality between the substrates (*vide infra*). Regardless of the origin, however, it is clear that sufficiently thin photoresist films free from metallizable defects can be fabricated on carefully selected substrates.

The selective attachment of a Pd catalyst to the SA film in the exposed and developed regions of the photoresist following development is a crucial step in the CCM process. This step must have a high degree of chemical selectivity to ensure that the following step of the process, EL metal deposition, will occur exclusively in the photoresist defined channels rather than on the photoresist. Therefore, the following experiments were designed to quantify the selectivity of attachment of **PD1** catalyst to a ligating SA film surface versus other surfaces in the CCM process using S1400 as the photoresist. Selectivity was evaluated using RBS, XPS, and EL Ni metallization. EDA-modified Si wafers were spincoated with S1400-17 photoresist and then processed with various combinations of UV exposure (254 nm lamp flood exposure for 2 sec), MF-312 (0.27 M) developer (70 sec), **PD1** (30 min), and 10% strength NIPOSIT® 468 plating bath at 25°C for 20 min. The process sequences were as follows: A) EDA/S1400/**PD1**; B) EDA/S1400/MF-312/**PD1**; C) EDA/S1400/UV/**PD1**; D) EDA/S1400/UV/MF-312/**PD1**. Results of the selectivity experiments are shown in Table 1 (next page). Si wafer substrates treated according to Processes B and D were analyzed by XPS. No detectable signal for Pd was observed for Process B, whereas the typical [11] Pd doublet (peaks centered at binding energies of 338 eV and 343 eV) due to **PD1** was observed for Process D.

These results show that the **PD1** catalyst is highly selective for the ligating SA film surface produced by exposure and development (Process D). There is essentially no binding to the surfaces

of the unexposed photoresist (Process A), the unexposed and developed photoresist (Process B), or the exposed and undeveloped photoresist (Process C). The previously determined [11] minimum Pd surface concentration (~1.1 x 10^{15} Pd(II) ions/-cm^2) required to initiate metallization is only exceeded when the resist is exposed and developed completely. These are also the conditions that yield homogeneous metallization using a Ni plating bath. The Pd surface concentrations determined by RBS that are in the ~10^{13} range are at the sensitivity limit of the instrument, and should be regarded as upper limits. Therefore, the selectivity of **PD1** catalyst binding to the exposed and developed EDA surface versus other surfaces is conservatively estimated at > 50-100:1.

Table 1. Catalyst and Metallization Selectivity

Process	Pd Concentration (atoms/cm^2)	Ni Plating
A	0.03 x 10^{15}	None
B	0.05 x 10^{15}	None
C	0.02 x 10^{15}	None
D	3.02 x 10^{15}	Complete

3.2 Lithographic Performance

3.2.1 Feature Density Dependent Metallization- The formation of the cleared channels through the photoresist following exposure and development is perhaps the most critical step in the CCM process. It is the stability and quality of the channel formed that will ultimately determine the fidelity of the pattern transferred into the substrate following the RIE. The pattern formed by the channel must correspond exactly with the image formed in the photoresist. This requires careful control of the processing conditions to ensure that the photoresist is correctly and completely exposed and developed through its entire thickness regardless of feature size or density. Incorrect exposure and development can lead to formation of non-vertical channel sidewall profiles and/or incomplete clearing in the channel. The former will lead to image distortion through fabrication of metal features whose dimensions do not correctly correspond to those of the original mask image, representing a loss of feature critical dimension (CD) control for the process. Incomplete clearing of the channel may inhibit subsequent catalysis and metal deposition, leading to formation of thinner metal structures that may fail during RIE pattern transfer. In more extreme cases, structures may only partially plate or not plate at all.

In the course of our initial experiments, however, we observed a dependence of metallization on feature density for the CCM process. The phenomenon manifested itself in terms of distinctly different exposure dose requirements for successful exposure, development, and metallization of densely versus sparsely packed features. In general, exposure and development conditions that led to uniform metallization of densely packed features inhibited or failed to initiate metal deposition in regions of low feature density. Adjustment of the exposure and development conditions to promote plating in the low feature density regions encouraged overdeposition of metal in the high density feature regions. The phenomenon was especially pronounced for positive tone photoresists.

Figure 3 (next page) provides an example of the feature density dependent metallization (FDDM) phenomenon using a system comprised of S1400 photoresist and EDA SA film as a model. Figure 3A shows densely packed branch structures correctly exposed, developed and plated with Ni according to the CCM process. For a positive tone photoresist such as S1400, the feature metallization bias is typically marked by an absence of plating at line ends and in isolated features in dark field (DF) regions. The effect is particularly severe for the rays of a DF Siemen's star feature. A

correctly plated Siemen's star, formed via metallization of a PEDA SA film directly patterned at 193 nm in the absence of photoresist [38], is shown for reference in Figure 3B. The convergence of metal rays comprises a region of high feature density near the center of the star and a low feature density region at the periphery. The corresponding star, formed using S1400 photoresist and the EDA SA film through the CCM process, is shown in Figure 3C. Although exposure, development, and plating conditions are identical to those used for the high density features of Figure 3A, metallization of the star is incomplete. Ni metal is selectively deposited in the channels corresponding to the densely packed features near the center of the star and extends outward along each ray. However, the deposited metal abruptly terminates after ~50-70% of the total length of the ray has been plated. The remaining portions of each ray comprising the lower density feature region near the periphery of the star remain unplated.

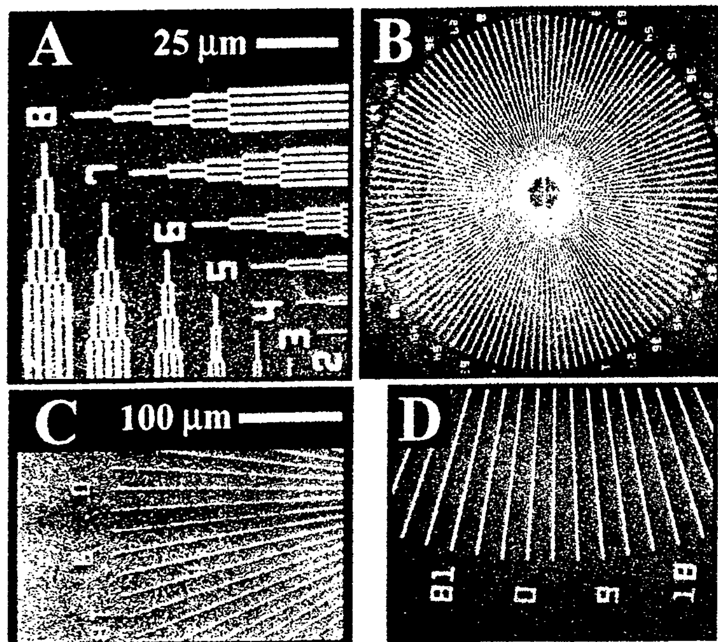

Figure 3. Micrographs of Low Resolution DF Ni Structures. (A) Ni branch structures; (B) Siemen's star with 2 µm width Ni rays formed by direct patterning of PEDA SA film on native oxide Si at 193 nm; (C) Siemen's star on S1400/EDA with partially Ni plated rays illustrating plating bias effect. The diameter of the star (excluding numbers) is 112 µm; (D) Clasp of Siemen's star edge showing completely plated rays and numbers. The distance between the tips of the rays labeled "18" and "81" is 26 µm. Ni plated areas are shown as light regions on all micrographs. Process sequences: (A)- S1400/EDA/Si (standard contact 365-405 nm exposure, 120 mJ/cm^2)/MF-312 (0.27 M, 90 sec) **PD1** (30 min)/10% NIPOSIT^R 468 EL Ni (20 min. 25°C)/Photoresist strip (acetone, 10 sec); (B)- PEDA/Si (193 nm ArF laser with contact mask, 900 mJ/cm^2)/**PD1** (30 min) 10% NIPOSIT^R 468 EL Ni (20 min, 25°C) [38]; (C)- Same as (A) except no photoresist strip; (D)- S1440/EDA/Si (standard contact 365-405 nm exposure, 150 mJ/cm^2)/ MF-312 (0.27 M, 120 sec) **PD1** (30 min)/10% NIPOSIT^R 468 EL Ni (20 min, 25°C) Photoresist strip (acetone. 10 sec).

To successfully practice the CCM process, it was clearly necessary to discern the nature of the FDDM effect and devise a practical solution. We therefore initiated experiments using the S1400/EDA DF Siemen's star of Figure 3 as a test feature to understand this phenomenon. The gradation from high to low feature density within each star provided an ideal medium for examination of the FDDM effect. Measurement of the fraction of each star ray plated proved a convenient means to quantify the degree of plating bias and measure our progress towards controlling the effect.

Although several hypotheses were considered to explain the FDDM effect, only two possibilities were consistent with the observed metallization bias effect. In the first, the source of the metal deposition bias involves the interaction of the EL bath with the feature to be plated. This model, known as the mixed potential theory (MPT), has been described in detail elsewhere in connection with EL metal deposition inside via holes [39, 40]. Metallization bias in this case is due to the breakdown at smaller, less densely packed features of the linear diffusional transport of EL bath components normally established during plating of larger or densely packed features. For

these smaller, more isolated features, mass transport by nonlinear diffusion is considerably enhanced compared to linear diffusion. The result is an increased flux of oxygen and EL bath stabilizer components to the feature site. Because oxygen reduction competes effectively with metal deposition over a wide range of solution pH, any enhancement of the local oxygen concentration at the feature due to nonlinear diffusion can effectively diminish plating. The concentration enhancement of EL bath stabilizers, which function as catalyst poisons, can likewise curtail or halt metal plating.

Systems in which the MPT mechanism dominates exhibit specific behavioral characteristics. For example, FDDM effects in such systems are typically diminished through the use of stronger, less stable EL metal baths. That is, increases in the deposition temperature, level of metal cation, and concentration of the reducing agent and/or decreases in the dissolved oxygen or stabilizer levels in the EL bath inhibit FDDM. The FDDM effect will be observed at low feature densities due to nonlinear diffusion processes even if the surface is adequately catalyzed, although increases in catalyst density or activity will again curtail the effect. Furthermore, the effect can also be quenched if isolated, low density features are electrically connected to a high feature density region. In this case, the plating potential at the isolated features is pinned to the steady state value established by linear reagent diffusion in the high feature density regions. Consequently, a potential favorable for metal deposition is established at the isolated feature sites despite the nonlinear diffusion effect.

We performed a number of experiments using the DF Siemen's star test structure to further examine the MPT hypothesis. Metallizations were performed using concentrated NIPOSIT® 468 EL Ni baths at elevated temperatures as well as baths in which the ratios of Ni(II), borane reductant and stabilizers were varied at room temperature and elevated temperatures. The effects due to dissolved oxygen were probed through experiments using nitrogen bubble degassed EL Ni baths. Additional experiments were performed in which the EDA SA film was replaced by a sputtered Pd metal film to (i) effectively increase the surface concentration of catalytic sites[2] for metal deposition in the channels following development and (ii) establish an electrical connection between the high and low feature density regions of the star. In each case, no significant diminution in the degree of plating bias of the star rays was observed. Further experiments in which stars were formed via direct patterning of the SA film and well catalyzed with **PD1** dispersion gave fully and selectively metallized stars (note Figure 3B) in contrast to the behavior predicted from the MPT mechanism. Consequently, the MPT mechanism appears to contribute little, if anything, to the FDDM effect observed in our systems.

An alternative possibility accounting for the observed metallization bias is insufficient local catalyst density and/or activity in the channels resulting from physical blockage of the ligand binding sites by photoresist residues. Physical blockage may be due to a variety of factors, including insufficient exposure (failure to expose the complete thickness of the photoresist) or incomplete development (failure to completely remove exposed photoresist from the channel). The presence of resist residues (*i.e.*, scum) in the channel may lead to chemical damage of the SA film ligand sites, reducing affinity of the catalyst for the binding site. Scum may also inhibit adhesion of the Pd(II) colloid particles to the surface, promoting non-uniform, lower coverage of the channel floor by the

---

[2] The use of a Pd metal surface rather than a SA film surface catalyzed by the **PD1** catalyst to initiate metal deposition leads to a > 10-fold increase in surface catalyst density. A 30 min treatment of the EDA SA film by **PD1** catalyst deposits ~1.7 x 10^{15} Pd(II) ions cm^{2} onto the film [11]. Following reduction, the number of Pd atoms available as clusters to act as catalyst sites is ~1.1 x 10^{15} Pd atoms/cm^{2}. For a continuous film of Pd metal, calculations using the density (~12 g/cm^3) and atomic weight (106.4 g/mole) of Pd metal indicate an effective surface concentration of ~16.6 x 10^{15} Pd atoms/cm^2.

catalyst.

In order to ascertain whether photoresist residues were present in the channels, we examined the Siemen's star of Figure 3C by AFM immediately after the photoresist development step but prior to catalysis or metallization. Figure 4A shows an AFM scan of a ray (channel) near the periphery of the S1400/EDA Siemen's star immediately after photoresist development; a close-up of the ray highlighting the edge of the channel is shown in Figure 4B. Although the channel step height of 1.1 μm is consistent with complete removal of the photoresist, the texture of the channel floor clearly indicates the presence of scum. The distribution of residue across the channel width is not uniform (note Figure 4B); scum deposition is heaviest near the walls and lightest in the channel center. There are obvious holes in the scum, especially in the center of the channel. Measurement of the hole depths provides an estimate of ~8-10 nm for the average thickness of the residue. Analysis of the AFM image indicates that the coverage of the ligand surface by residue particles is at least 70%. The quantity of scum in the channels decreases markedly upon approaching the center of the star. The surface coverage by residues in the high density features near the star center is < 5%.

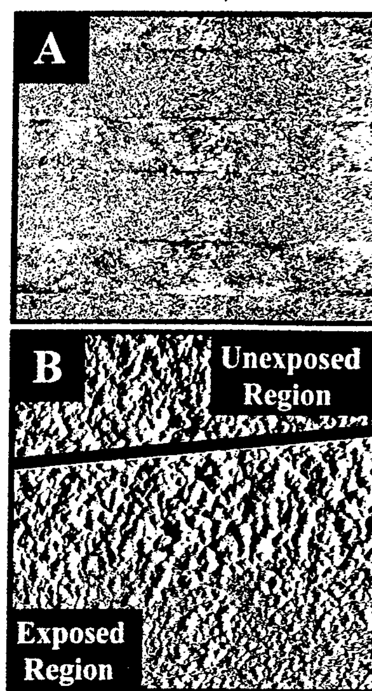

Figure 4. Tapping Mode AFM of the Siemen's Star. (A) AFM image of Siemen's star ray on S1400/EDA/Si after exposure and development but prior to catalysis or plating as described for Figure 3C (field size 15 μm x 15 μm); (B) Close-up of the star ray in part A (field size 2 μm x 2 μm). The black line represents the channel wall boundary; the upper portion is unexposed and undeveloped S1400 photoresist and the lower portion shows the developed channel floor. Note the presence of residue particles in the channel.

The partially metallized star of Figure 3C was also examined by AFM and Auger Electron Spectroscopy (AES) to identify the materials present in the star rays after catalysis and metallization. An AFM examination of the portion of the rays nearest the center of the star (light regions, Figure 3C) indicated the presence of an ~40 nm thick layer of material. This material was subsequently identified as Ni metal by AES. AFM examination of those portions of the rays near the star periphery again revealed residues in the channel. However, the thickness of the residues had increased to ~15-20 nm, consistent with the deposition of additional materials during catalysis and metallization. The AES profile indicated that the additional residue consisted of Pd; no Ni was observed in these areas as expected from the metallization behavior (Figure 3C).

The results of the AFM and AES experiments strongly support a model in which accumulation of residues in the channels of the low density features physically blocks the ligand sites. Effective surface catalyst densities are readily estimated using the coverage results from the AFM experiments and provide additional support for the model. For stars formed by direct patterning of the SA film (e.g., Figure 3B), no residues are deposited and complete metallization occurs. For a typical catalysis time of 30 min using **PD1** catalyst, ~1.7×10^{15} Pd(II) ions/cm^2 are deposited in this case onto the ligand surface [11]. Because this value exceeds the minimum catalyst density required to initiate and sustain EL Ni deposition (~1.1×10^{15} Pd(II) ions/cm^2) [11], selective plating occurs.

For the S1400/EDA star of Figure 3C, however, the density of available ligand sites in the ray channels near the edge of the star is reduced ~70% by residues to a first approximation. A corresponding reduction in catalyst level is equivalent to an effective surface coverage in the channel of ~0.5×10^{15} Pd(II) ions/cm^2. Metallization cannot be initiated at this sub-critical catalyst density. In contrast, because scum covers < 5% of the channel floor in the higher feature density regions near the star center, the effective catalyst density in the channels remains well above the threshold and plating occurs.

Our results clearly indicate that selective metal deposition in the photoresist channels defining a pattern can be achieved, provided that channels are free from residues following development. Defining proper exposure and development conditions that minimize scum deposition is therefore an important issue for successful practice of the CCM process. A prerequisite for accomplishing this task is an understanding of the nature and source of the residue. Fortunately, both the composition of deposited residues and their formation mechanism in positive tone photoresists such as S1400 have been determined [41, 42]. Residues consist of two components. The minor component contains diazo-crosslinked polymeric species formed by attack of the DNQ diazo group on the novolak phenol side group during the PAB step. The major component has been shown to consist of the less soluble tris-cresol DNQ ester from the mixed cresol DNQ esters comprising the PACs of the photoresist.

The difference between the exposure doses required to clear the high and low feature density regions sufficiently to permit metallization indicates an important role for light in scum formation. During patterning, light penetrating the S1400 photoresist will reflect and scatter from the underlying substrate as the exposure progresses.[3] The reflected light will contribute to the exposure of the photoresist. The contribution from this effect will be more pronounced in high feature density regions, given the greater effective light flux entering the photoresist in these areas compared to the low feature density regions. Therefore, the exposure time (*i.e.*, effective dose) required to fully convert the DNQ groups of the photoresist PACs to the corresponding indene carboxylic acids will be greater in the low feature density regions than in the high feature density regions. Consequently, at an exposure dose appropriate for printing high density features, some fraction of the PACs in the lower feature density regions will remain unconverted to carboxylic acid photoproduct. These less soluble PACs (*i.e.*, unreacted tris-cresol DNQ esters) accumulate as scum in the channels of the low feature density regions during development as the more soluble photoresist components are carried away in the developer solution [41, 42]. If the dose is adjusted to fully expose the low feature density regions, the corresponding increase in scattered/reflected light in the high feature density regions will overexpose these areas. In this case, somewhat broader channels than anticipated will be produced following development and loss of feature CD control will occur if the degree of overexposure is sufficiently large. In the most severe cases, complete pattern degradation due to thinning and collapse of channel walls would result, leading to complete overmetallization of the substrate. This latter concern is most important for higher resolution features and is discussed in greater detail in Section 3.2.3.

Our observations concerning the scum suggested that a simple strategy involving slight overexposure of the high density feature regions combined with more aggressive development should

[3] A case for negative tone photoresists will be considered in connection with printing sub-micron features in Section 3.2.2.

minimize the level of deposited residues while maintaining adequate feature CD control. We tested this strategy through variations of the exposure dose and development conditions during fabrication of metallized S1400/EDA Siemen's star patterns. The branch structures from Figure 3A served as a model for successful plating of densely packed features; such features were correctly plated following exposure at 120 mJ/cm^2 and development for 90 sec in 0.27 M MF-312 developer solution. For an identically processed Siemen's star, the average percentage of each star ray plated was 72 $\pm$ 13% due to the FDDM effect. As expected, at a dose of 150 mJ/cm^2, more complete exposure of the photoresist in that portion of the rays near the star edge (*i.e.*, low feature density regions) improved clearing during development, raising the plating percentage to 90 $\pm$ 4%. Plating of 92 $\pm$ 3% of each ray could likewise be achieved at a dose of 120 mJ/cm^2 if the development time was increased to 120 sec. Unfortunately, more aggressive development regimens were unsuccessful in completely clearing the photoresist from the entire ray for stars exposed at 120 mJ/cm^2. For example, use of surfactant-containing MF-319 developer in place of the otherwise equivalent MF-312 solution gave no improvement in metallization of the star rays. Attempts to fully develop the patterns at elevated temperatures (*e.g.*, 50°C) or in an ultrasonic bath promoted lift-off of the S1400 photoresist from the EDA SA film. However, through mild overexposure at 150 mJ/cm^2 of the densely packed features comprising the center of the star in conjunction with a 30 sec extension in development time to 120 sec, plating of 99 $\pm$ 2% of each ray was finally achieved with adequate feature CD control. A close-up view of the ends of the rays of a properly plated star is shown for reference in Figure 3D.

3.2.2 High-resolution Features- The challenges associated with the clearing of residues for DNQ-based positive tone photoresists clearly limits their effectiveness as imaging systems for the CCM process. Masks used for IC fabrication may contain a wide range of structures of various sizes, shapes, and tones that must all be properly printed. Areas consisting of largely metal covered regions in which openings in the metal define the features (dark field, DF) may exist near largely transparent regions in which the metal itself represents the pattern (bright field, BF). Local areas in which features of higher or lower densities coexist may be found in each region (*e.g.*, note DF features from Figure 3). The variances in light flux inherent in such designs pose a severe challenge in the application of the aggressive development protocol for the fabrication of metal features. As the degree of divergence in feature size and density increases on a given mask, a point will be reached where both BF and DF metal features cannot be simultaneously printed with adequate feature CD control. For example, attempts to correctly print slightly overexposed BF features will require extremely harsh development conditions to remove the underexposed photoresist in the DF regions. The extreme development conditions necessary to remove residues in the DF features will result in overdevelopment of the BF features, creating unacceptably broadened and distorted channels. Such problems will be compounded for higher resolution features by the requirement to remove scum from the narrower channels defining the features. In addition, photoresist lift-off leading to pattern degradation may well be promoted due to further narrowing of necessarily small feature channels during development.

Given the potential complications arising from residue formation associated with use of positive tone photoresists, we examined negative tone photoresists as alternative imaging layers for sub-micron resolution features. Residue formation was expected to be less of a concern in these chemically-amplified systems due to differences in composition and patterning mechanism compared to their positive tone analogs [34]. Whereas irradiation increases solubility of the positive tone resist, it initiates a polymerization in chemically-amplified negative tone photoresists that hardens the

irradiated area (eqs 1-3, Scheme 1). Development therefore dissolves the unirradiated areas of the negative tone resist. Because the lower molecular weight novolaks, crosslinker and PAG present in the negative tone resist prior to irradiation (*vide supra*) are typically more soluble species than the corresponding PACs from positive tone resists, scum formation was thought to be less likely to occur. Consequently, we examined various combinations of negative tone resists and SA films to better evaluate the ability to fabricate sub-micron features using the CCM process. The questions of interest are identical to those posed for the positive tone systems. That is, are exposure dose and metallization bias effects observed with these systems and, if so, are residues responsible for the effect? Furthermore, if residues are present, what are their mechanisms of formation and interaction with the SA film and how might their influence in the CCM process be ameliorated?

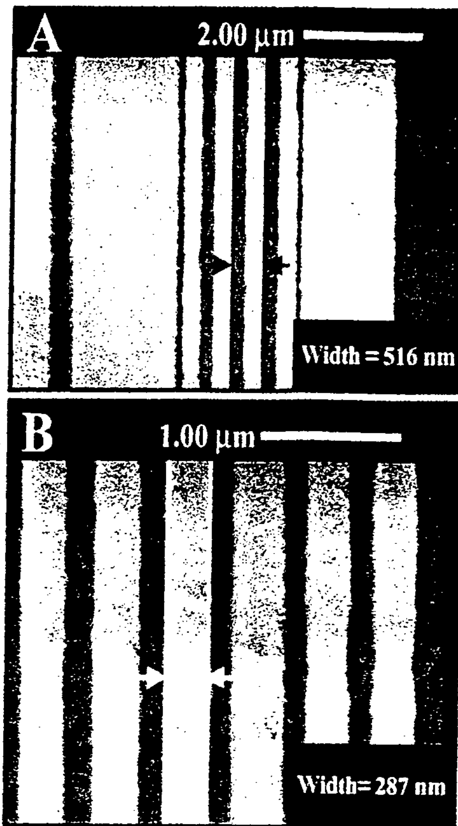

Figure 5. Scanning Electron Micrographs of Equal Line/Space Gratings on SNR-200.5/PHOS/Si. (A) DF 0.25 μm Ni (light areas) gratings; (B) Nominal 0.25 μm BF Ni (light areas) gratings measuring ~0.29 μm wide. Process sequence for (A) and (B): DUV projection stepper (248 nm, 0.53 NA, 23 mJ/cm^2)/ PEB (120°C, 90 sec) CD-14 (40 sec)/**PD2** (10 min)/ 10% NIPOSIT[R] 468 EL Ni (10 min, 25°C)/SO_2-O_2 plasma etch (note Experimental) [31].

Exposure and metallization bias effects, which plague the positive tone photoresist systems, are indeed also found using negative tone photoresists in the CCM process.[4] Figure 5 shows grating structures formed using SNR-200.5 negative tone photoresist and PHOS SA film exposed with a DUV stepper after development and metallization. Figure 5A shows Ni metallized nominal 0.25 μm DF gratings patterned at a dose of 23 mJ/cm^2. The gratings printed measure 0.25 μm, although some narrowing of the gaps at the edges compared to the middle of the pattern due to optical proximity effects in the resist are observed. The corresponding BF gratings fabricated under identical conditions are shown in Figure 5B. Unequal lines and spaces are observed, consistent with underexposure and subsequent erosion of the channel walls during development. Metallization occurs in broadened channels, leading to measured linewidths of 0.29 μm for the nominal 0.25 μm features. This increase in linewidth signifies a loss of CD control that must be addressed if the CCM

[4] Note that the DF and BF features exposure bias is an inherent feature of photoresists. For single level lithography systems, in which the photoresist functions as both imaging layer and plasma etch resistant mask for pattern transfer, there is no need to completely clear channels during development. Minor quantities of residue can be effectively removed using a brief O_2 plasma descum without materially affecting the ability of the remaining photoresist to function as an effective plasma etch resistant mask during the subsequent RIE pattern transfer step. Consequently, exposure and development process latitudes are sufficiently large to permit adequate processing of most features regardless of size and/or density. For the bi-level CCM process, however, a plasma descum cannot be used to remove residues without also removing the ligand SA film required for metal deposition. The requirement that scum be removed solely through adjustment of the exposure and development conditions imposes additional challenges concerning feature CD control in the case of the CCM process compared to single level lithographies.

process is to be used to reliably fabricate sub-micron features.[5]

Underdosed SNR-200.5/PHOS BF gratings can be properly printed by increasing the exposure dose. Figure 6 shows the bank of BF 0.24-0.20 μm gratings exposed at 36 mJ/cm^2 following Ni plating. BF 0.24 μm grating structures with nominal 0.24 μm gratings are measured as 0.24 μm. The Ni gratings extend to 0.20 μm, consistent with the resolution limit of the photoresist. However, analogous banks of DF gratings are not plated under these conditions. In fact, plating occurs only for DF gratings having feature dimensions of 0.37 μm or greater under these conditions.

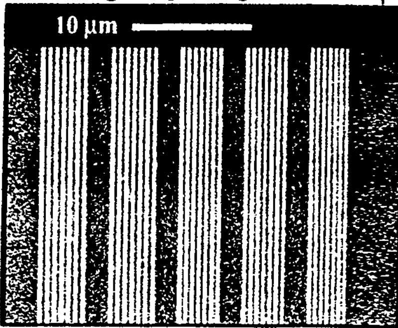

Figure 6. Scanning Electron Micrographs of BF Ni Gratings on SNR200.5/PHOS/Si. Equal line/space Ni (light areas) gratings of sizes (left to right) 0.24 μm to 0.20 μm in 0.01 μm steps. Process steps are equivalent to those described in Figure 5 except an exposure dose of 36 mJ/cm^2 was used.

To determine the origin of the metallization bias in this system, we examined 0.31-0.39 μm banks of DF gratings after development but prior to catalysis or metallization. Figure 7A (next page) shows an SEM of SNR-200.5/PHOS DF nominal 0.33 μm gratings exposed at 40 mJ/cm^2 and developed 40 sec with CD-14. Under these exposure and development conditions, gratings of 0.33 μm size (*vide infra*) remained unplated following treatment with catalyst and EL bath. Although the two leftmost trenches appear to be residue free, scum is clearly observed in the remaining channels. This behavior clearly indicates that physical blockage of the channels by residues does contribute, at least in part, to the inability to metallize these features.

Plating failure in the apparently clear channels in Figure 7A raised the possibility that a mechanism in addition to simple physical blockage could contribute to inhibition of metal deposition in these systems. However, possible alternatives were readily dismissed after considering the behavior of the system further. For example, plating failure due simply to an inability to transport sufficient catalyst or EL bath into the small, hydrophobic resist channels during the times allotted for these steps was inconsistent with our ability to plate the higher resolution features of Figure 7.[6]

[5] The potential distortion of features produced using the aggressive development strategy has already been noted in connection with the fabrication of lower resolution structures, such as the Siemen's star of Figure 3C, using positive tone photoresists in Section 3.2.1. As feature resolutions increase, however, the ability to control variations in feature linewidth becomes increasingly more difficult. For example, although a 0.04 μm change in linewidth constitutes only a 2% error in the 2 μm width of the Siemen's star ray, the same variance represents a 16% deviation for a 0.25 μm feature. Although the former value is well within the 10% tolerance guidelines specified by IC design rules, the latter value is not. Consequently, larger absolute variations in linewidth can be tolerated within the design rule restrictions for lower resolution features. This permits use of somewhat greater exposure/development process latitudes for the lower resolution systems.

[6] The times required to wet features and transport materials from bulk solution to the channel floors [43], as well as the concentration profiles of EL bath components in a feature channel [44], are readily estimated. Reference 43 describes the surface water drop contact angle (θ_w) dependence of both feature wetting time (eqs 1 and 9) and the time to transport a chemical species into a feature channel from bulk solution (eq 11) for features of various widths and aspect ratios. For typical hydrophobic photoresist films with θ_w ~70°, wetting of a 0.10 μm width channel of depth 1 μm is complete within 2-3 seconds. Furthermore, the concentration of a reagent such as **PD1** catalyst at the channel floor attains 99% of its concentration in bulk solution within ~1 sec. These timescales are far too short compared to our minimum catalysis (2 min) time to effectively hinder catalysis in our systems. Analogous calculations for metal deposition, which must consider the continuous growth of metal within the channel, are discussed in reference 44. For conformal metal filling (*i.e.*, growth

Chemisorption of photoresist to the ligand SA film represents another potential means through which plating may be inhibited. In this mechanism, diffusion of acid from protonated ligand sites on the SA film into the photoresist would catalyze formation of alkylating agent (eq 2, Scheme 1) in the interfacial region during PAB or PEB. Initial alkylation of the ligand functional group followed by subsequent alkylation of photoresist (eq 3, Scheme 1) would covalently bind the resist to the SA film. The resulting chemical changes and/or steric effects would render the ligand incapable of binding sufficient catalyst to initiate metal deposition.

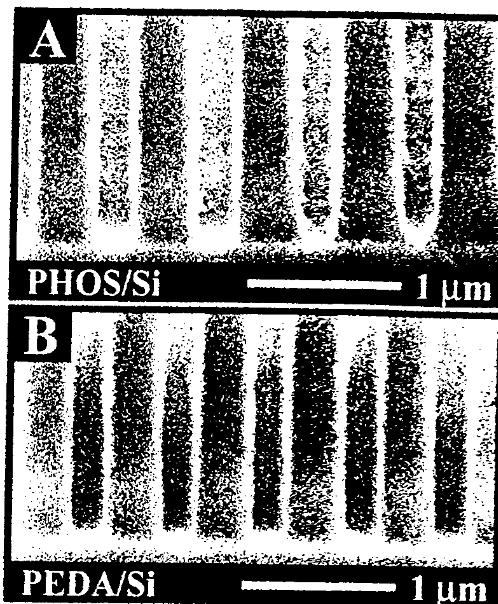

Figure 7. Scanning Electron Micrographs of Developed Photoresists. (A) Nominal 0.33 µm SNR200.5/PHOS/Si; (B) Nominal 0.31 µm SNR200.5/PEDA/Si. Process sequence: DUV projection stepper (248 nm, 0.53 NA, 40 mJ/cm^2)/PEB (120°C, 90 sec)/CD-14 (40 sec).

The chemisorption possibility was tested through preparation of a pattern of SNR-200.5/PEDA DF gratings under conditions identical to those used to prepare the bank of SNR-200.5/PHOS gratings of Figure 7A. The PEDA SA film is more readily protonated than the corresponding PHOS film (note pK_a's in Figure 2). In addition, the less hindered, more nucleophilic N sites of the PEDA are more easily alkylated than the P site in PHOS. Consequently, the thermal binding reaction, if it occurs, should proceed more rapidly and completely at the PEDA sites than the PHOS sites. The SEM of the SNR-200.5/PEDA DF gratings shown following development in Figure 7B is not consistent with these expectations. In contrast to the SNR-200.5/PHOS system shown in Figure 7A, all channels are apparently free from residues. In addition, treatment of the SNR-200.5/PEDA sample with catalyst and NIPOSIT® EL Ni bath does lead to selective Ni metallization of the entire grating structure (*vide infra*, Section 3.2.3). These results suggest that chemisorption of resist to the ligand SA film, if it occurs at all, is not sufficient to appreciably affect subsequent catalysis and metallization of in the photoresist channels. Consequently, the inability to plate the SNR-200.5/PHOS channels in Figure 7A is most consistent with a failure to completely remove physisorbed, rather than chemisorbed, residues during development.

The accumulation of residue at the base of the channel walls in Figure 7A suggests a residue formation mechanism in which light scattered into the masked regions of the photoresist during

---

of metal from both the channel floor and walls), the concentrations of EL bath components at the channel floor relative to their values in bulk solution are functions of diffusivity and plating rate. The concentration is directly proportional to a component's diffusion coefficient (D) and inversely proportional to plating rate under steady state conditions established during plating. For a species such as Cu^{2+} (or Ni^{2+}) with typical D ~10^{-5} cm^2/sec and a plating rate of ~300 nm/h, the metal cation level on the floor of a 0.10 µm wide channel of depth 1.5 µm is maintained at ~99% of the bulk value throughout the deposition process. In our process, plating originates only on the channel floor and proceeds at a rate ≤ 100 nm/h. Consequently, this value represents a lower limit for our system. EL bath components are therefore maintained at near bulk solution values on the channel floors during plating of our features.

exposure promotes acid generation required for the formation of the physisorbed residues during the PEB.[7] Because scattered light will increase proportionately with dose, so too must the quantity of residue formed in the feature channels during PEB and development. Eventually, the amount of residue formed will reach a critical value as dose is increased. This critical value corresponds to the maximum quantity of residue that can just be completely removed from the channel for a fixed set of development conditions. If the quantity of residue formed exceeds this threshold, sufficient scum will remain on the channel floor to block metal deposition. Thereafter, continued irradiation (*i.e.*, overdosing) will no longer impact the ability of the feature to metallize. However, sufficient quantities of residue will eventually be generated to exceed the threshold values for larger (*i.e.*, lower resolution) features. Consequently, the feature size at which metal deposition cuts off should vary monotonically with dose (*i.e.*, scattered light) within a series of geometrically identical structures of varying linewidth subjected to a fixed development regimen.

We tested this model by measuring the feature size plating threshold as a function of exposure dose for a bank of DF SNR-200.5/PHOS grating structures with linewidths between 0.80-0.20 μm. Following exposure at 248 nm using the DUV stepper and PEB, samples were identically developed for 40 sec using CD14 developer, catalyzed 10 min using **PD2**, and plated for 10 min at room temperature in 10% NIPOSIT® 468 Ni bath. At 23 mJ/cm^2, gratings with resolutions between 0.80 μm and 0.25 μm are selectively plated; features of dimensions 0.24-0.20 μm remain unplated. Increasing the delivered dose to 35 mJ/cm^2 raises the metallization threshold to 0.37 μm. Minimum linewidth Ni gratings are observed at 0.43 μm as the dose is further increased to 40 mJ/cm^2. At 50 mJ/cm^2, the metallization threshold is 0.60 μm and only those gratings of size 0.60-0.80 μm plate. This behavior, representing a nearly linear increase in plating threshold with dose, corresponds exactly to that predicted from the model and provides strong support for the role of scattered light in the creation of scum in these systems.

3.2.3 Adhesion- The observation of residues in the channel trenches of Figure 7A once again suggests adoption of an aggressive development protocol, as described for the lower resolution Siemen's star feature of Figure 3C, as a viable strategy for scum removal. For sub-micron features, however, overdevelopment must be employed with caution. Excess development can erode channel walls, especially for underdosed features, leading to loss of feature CD control during metallization (note Figure 5B). In addition, photoresist lift-off may occur if the adhesion of the photoresist to the ligand SA film is sufficiently compromised by the treatment conditions.[8]

---

[7] An alternative mechanism for scum formation involves diffusion of acid generated in the irradiated portions of the photoresist into the masked regions during PEB. However, this mechanism can be dismissed given the limited mean free path of only ~7 nm determined for diffusion of the H^+ in the photoresist during the PEB step [34].

[8] At least two factors contribute to adhesion loss. Consider a set of gratings such as those shown in Figure 7. Let "x" describe the width of a resist post comprising the grating. Let "y" be its depth (*i.e.*, length) and "z" its height. The effective footprint of the post in contact with the substrate has area, "xy". As the feature resolution increases, the area "xy" decreases and so too will the number of interactions (*i.e.*, adhesive force) anchoring the post to the substrate. Defects in the interfacial region between the photoresist and the substrate will also become increasingly important. During development, migration of developer into the interface through defects will further diminish the adhesive force [45-47]. In addition, shear forces created by agitation (stirring) of the developer solution will act on the exposed faces of the post. At high resolution (*i.e.*, smaller "x"), the force will act primarily on the channel walls. Because the area of the channel walls, "yz", does not change with feature resolution, a constant torque will be applied to the post. A critical value of feature width, "x_0", will eventually be reached at which the adhesive force just balances the torque and the influence of the developer penetrating the interface. The adhesive force, and therefore "x_0", will depend upon the nature of the photoresist-

Figure 8 illustrates the consequences of adhesive failure of the photoresist film in the CCM process using SNR-248 negative tone photoresist and the EDA SA film. In this system, high-resolution (0.80 µm) regions in the exposed and developed photoresist clearly exhibited curved and collapsed structures indicative of photoresist lift-off and redeposition on the SA film. Nevertheless, the wafer was catalyzed and Ni was plated for several hours to build up thicker than usual Ni deposits in the channels. The channel-constrained metal followed and effectively mapped the contours of the collapsed photoresist template to produce the curved ~0.80 µm wide structures of Figure 8A. The poor adhesion of the SNR-248 photoresist to the EDA SA film is further illustrated in Figure 8B by the thin metal "feet" that extend from the base of the Ni line into the region that should have been blocked by the photoresist. However, it should be noted that even this experiment highlights the ability of the CCM process to produce high aspect ratio structures with relatively smooth edges due to the channel-constrained buildup; the Ni lines of Figure 8B are 0.35 µm wide and nearly 0.70 µm thick.

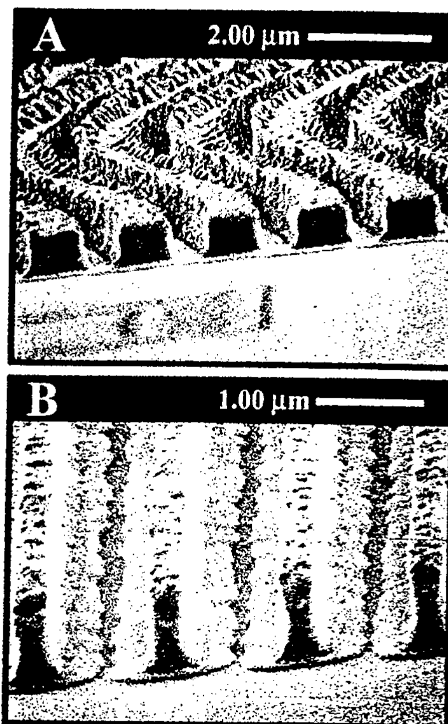

Figure 8. Adhesive Failure of Photoresist in the SNR-248/EDA/Si System. Scanning electron micrographs of Ni features formed after extended plating of (A) photoresist gratings that had partially lifted off and redeposited during development, and (B) photoresist gratings that had been incompletely undercut during development. Process sequence: DUV projection stepper (248 nm, 0.53 NA, 14 mJ/cm^2) PEB (100°C, 1 min)/XP89-114 developer (2 min)/**PD1** (30 min)/ 10% NIPOSIT® 468 EL Ni (24 h, 25°C) /XP91140 photoresist remover (1 min).

The pattern lift-off associated with insufficient photoresist-substrate adhesion can be eliminated through proper choice of photoresist and SA film. For example, adhesion of SNR-200.5 photoresist to the SA films used in these experiments is found to increase in the order EDA < PYR < PHOS ≤ PEDA. This order parallels the hydrophobicity (as measured by θ_w from Figure 2) of the ligand and suggests that in this case van der Waals, rather than covalent,[9] interactions predominate at the photoresist-substrate interface. The adhesion of SNR-200.5 to PEDA is somewhat stronger than its adhesion to PHOS. Whereas the SNR-200.5/PHOS system is sufficiently adhesive to tolerate CD14 development for 40 sec, partial lift-off occurs if development is extended to 60 sec to clear the channel residues in Figure 7A. In contrast, the corresponding SNR-200.5/PEDA system of Figure 7B does withstand the 60 sec development. This behavior is consistent with previous studies in which proper surface energy matching of substrates ($\theta_w \geq 60°$) and photoresists ($\theta_w \sim 65$-$75°$) has been identified a prerequisite for adhesive contact [46, 47].

Adjustment of the photoresist-substrate adhesion promotes plating of sub-micron features

substrate interactions [48-51]. If "x" is reduced such that it becomes smaller than "x_0", the applied torque will overwhelm the adhesive force and lift-off of the post will occur.

[9] The same argument made in Section 3.2.2 with regard to residue chemisorption to the ligand sites of the SA film in masked regions of the pattern applies in connection with resist adhesion in irradiated regions.

with good feature CD control using the CCM process. Figure 9A shows a DF grating bank identical to that containing the nominal 0.31 μm SNR-200.5/PEDA structures from Figure 7B following Ni metallization. Metal gratings in the size range 0.39-0.31 μm formed following a 41 mJ/cm^2 dose and 40 sec development are fully and selectively metallized. A second bank of gratings (not shown) comprising lower resolution (*i.e.*, 0.80-0.41 μm) structures is also plated. The corresponding banks of BF gratings, identically exposed and developed, are similarly plated. A close-up view of the plated 0.39-0.31 μm BF gratings is shown in Figure 9B. Feature CD control for the SNR-200.5/PEDA gratings is good; nominal 0.50 μm and 0.33 μm Ni gratings are measured as 0.50 μm and 0.32 μm, respectively. In fact, the increased exposure/development process latitude afforded by the improved adhesion in this system allows plating of still smaller features via additional development. For example, at an exposure dose of 36 mJ/cm^2 and a 60 sec development time, features to 0.25 μm resolution are successfully plated. Consequently, through maximization of photoresist-substrate adhesion, printing of a range of both DF and BF high-resolution metal features at a single exposure dose with acceptable feature CD control is achieved.

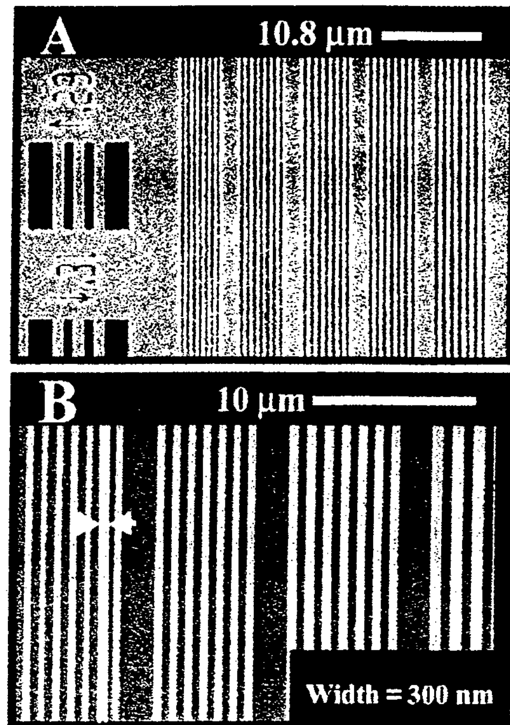

Figure 9. Scanning Electron Micrographs of Equal Line/Space Ni Grating Blocks on SNR200.5/PEDA/Si. (A) Overview of DF blocks showing Ni plated (light areas) gratings ranging (left to right) from 0.31 μm to 0.39 μm in 0.02 μm steps; (B) Close-up of BF Ni blocks (light areas) with gratings ranging from (left to right) 0.31 μm to 0.37 μm in 0.02 μm steps. Process steps are equivalent to those described in Figure 5 except an exposure dose of 41 mJ/cm^2 was used.

3.2.4 Pattern Transfer- The final lithographic step in the CCM process comprises the reactive ion etch (RIE) for pattern transfer into the substrate. Several requirements must be met in order for a material to qualify as an acceptable etch mask [33, 52]. First and foremost, the material must exhibit a high resistance to degradation when exposed to plasmas typically encountered during the microelectronics pattern transfer process; these include fluorine-based plasmas for Si/SiO_2 etches and/or O_2 plasmas for polymer planarizer substrate etches. Furthermore, the mask material must selectively deposit on each feature at a sufficient thickness to (i) withstand plasma degradation during the time required to achieve the desired feature etch depth, and (ii) heal pinholes that might otherwise degrade the structure during the etch process. The mask thickness should be uniform across the feature width regardless of feature size, geometry or density on the substrate. The mask edge must correspond precisely with the feature edge throughout the entire thickness of the mask (*i.e.*, a vertical sidewall is ideally maintained in the mask material) to prevent feature linewidth erosion during the plasma etch. In addition, the deposition process for application of the etchmask must be compatible with standard track operations routinely employed during IC fabrication.

We performed a number of experiments that clearly demonstrated the fitness of deposited metal films as plasma etchmasks and the unique advantages that accrue with their use in the CCM

process. For example, the issue of adequate metal mask deposition selectivity has been previously demonstrated in connection with our discussion of catalyst selectivity in Section 3.1.2. Furthermore, because the metal mask growth occurs within the constraints of the feature channel walls, lateral metal growth that might otherwise contribute to a loss in feature CD control is arrested. The dimensions of the metal film and its sidewall profile conform to the cross-section of the channel defining the feature as required to faithfully transfer the pattern into the substrate during the RIE.

The efficacy of EL Ni films[10] as masking layers for pattern transfer into Si was illustrated by etching metal patterned wafers in a mixture of SF_6 and CHF_3 for varying times. Figure 10A (next page) shows a 2 μm Ni grating after etching to a depth of ~3.3 μm into the Si substrate. The original thickness of the Ni etchmask was ~30 nm. The Ni films in Figure 10A appear uniform[11] and exhibit no apparent Ni loss following the etch; line edge roughness is ≤ 10 nm and no noticeable erosion of feature linewidths is observed. Near vertical sidewalls are maintained for the high aspect ratio (1.65) structures, consistent with requirements for effective pattern transfer (*vide supra*).

In contrast, Figure 10B shows an isolated 4 μm Ni line from the same sample following etching to a depth of ~4.4 μm into the Si substrate. Although the vertical sidewall profile is maintained and no apparent linewidth erosion or loss of edge acuity of the feature is observed, obvious roughening of the Ni etchmask has occurred. In addition, some fraying of the Ni film at the

---

[10] There are two important concerns with respect to the use of metal etch masks in IC fabrication. The first involves the potential for formation of deep level traps due to diffusion of certain metal ions into the Si during processing that can ultimately render an IC inoperable. Although Ni ions can form such traps, other metals [6] such as Co or Cu that can be electrolessly plated are already used in IC device fabrication and may be less objectionable. A second concern involves completion of the metal deposition within the allowable process step time (~2 min) during device fabrication. A 10 % strength EL NIPOSIT® Ni 468 bath typically deposits Ni at a rate of ~1.5-2.0 nm/min at room temperature onto SA films catalyzed using **PD1** or **PD2** during the first ~30 min of plating. The 30 nm thick Ni film is therefore formed after ~20 min of plating. Because the plating rate increases with concentration and temperature, the time required for deposition of an acceptably thick Ni film can be appreciably reduced. For example, a plating rate of ≥ 15 nm/min is obtained using a full strength bath at 60°C. Consequently, the same 30 nm thick Ni film can be deposited in the required 2 min time interval under these conditions.

[11] We directly measured the uniformity of metal deposition for features of various sizes, geometries and densities using stylus profilometry for low resolution (*i.e.*, ≥ 1 μm) structures fabricated using S1400/EDA. Efforts to measure sub-micron features in this manner were not attempted given the size of the tip (2-5 μm) relative to the feature dimensions. Various DF and BF metal features were examined, including 5 μm branch structures (*e.g.*, Figure 3A), the 2 μm Siemen's star rays (*e.g.*, Figure 3D), individual 2 μm lines from banks of gratings, and isolated 1 μm lines. Average metal thicknesses (4 measurements per structure) for the DF features were 55 ± 5 nm, 53 ± 4 nm, 52 ± 3 nm, and 53 ± 4 nm, respectively. Values for the corresponding BF versions of each feature were 44 ± 4 nm, 40 ± 4 nm, 49 ± 5 nm, 49 ± 4 nm, respectively. These results are indicative of good uniformity in metal deposition for features within a given field (*i.e.*, BF vs. DF). The observed variations in metal thickness for a given feature and the apparent bias towards thinner plating for BF features are due, at least in part, to two factors. First, platings were performed with manual agitation of the solution: lack of automated processing during this critical step is certainly expected to influence reproducibility. In addition, the stylus profilometry measurements used to determine metal thickness are influenced by the convolution of the tip (2-5 μm radius) with the features, even for these lower resolution features. For the DF structures, convolution is minimized because the tip travels from a well-defined baseline in the unplated field up and over the metal feature and back down to the field. In contrast, the steric interaction between tip and sample is greater for BF structures because the tip must travel from a plated mesa down into a narrow trench and back up to the mesa. Consequently, measurements made for the BF features are biased towards lower apparent thickness values than the corresponding DF measurements.

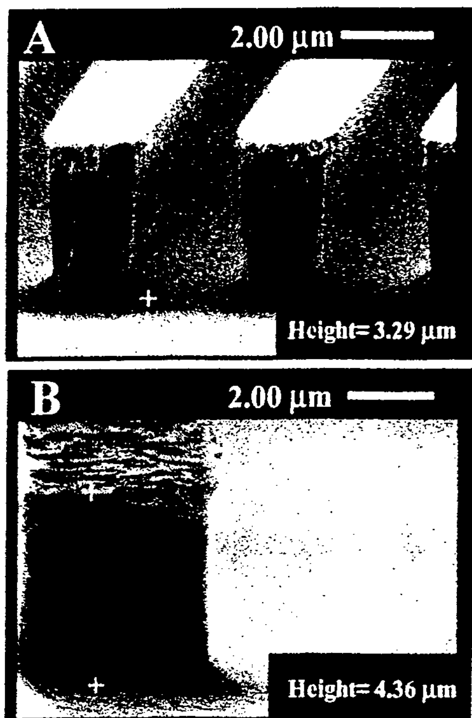

Figure 10. Scanning Electron Micrographs of High Aspect Ratio Etched BF Ni Structures. (A) Equal line-space 2 µm Ni gratings; (B) Isolated 4 µm Ni line. Process steps: S1400/EDA Si (standard contact 365-405 nm exposure, 120 mJ/cm^2)/MF-312 (0.27 M, 90 sec)/**PD1** (30 min)/10% NIPOSIT® 468 EL Ni (20 min, 25°C)/Photoresist strip (acetone, 10 sec) RIE (SF_6-CHF_3 plasma, note Experimental)

feature edge consistent with partial erosion of the metal etchmask is evident. Additional erosion of the masking layer occurred as etching was continued, leading eventually to roughening of the Si surface and observation of an essentially constant trench depth. The 30 nm thick Ni etchmask yielded maximum etch depths of 6-8 microns before breakthrough, giving an estimated selectivity of at least 200:1 vs. Si. Similar selectivity values have been calculated for metal features prepared by direct plating of scanning tunneling microscope (STM) imaged surface ligands in the absence of photoresist [21, 22], consistent with the expected lack of influence of the photoresist topography on the ligand SA film reactivity within the channel [43, 44].

Ni films were also evaluated as etchmasks for pattern transfer through polymer planarizer films using O_2 plasmas. Figures 11A and 11B (next page) show Ni star and high resolution isolated line structures formed following 13.4 nm EUV exposure, development, Ni deposition, and etching of ~68 nm thick SAL-601-ER7 photoresist on EDA-modified S1400 crosslinked planarizer films. With technologies such as EUV lithography, where highly attenuated radiation can yield nonvertical photoresist channel sidewall slopes, producing an etchmask of the minimum possible thickness is important. Variations in thickness, both above and below the minimum value, would be detrimental to the process, leading to either ineffective etch masking or loss of linewidth CD control.

Recent work in our group indicates that Ni films as thin as ~8-10 nm can provide sufficiently homogeneous, pinhole-free masks for acceptable pattern transfer via RIE [53, 54]. We therefore tested Ni masks of this thickness in Figure 11 for pattern transfer of the EUV exposed samples. Examination of the Ni lines in Figure 11B indicates that measured linewidths are somewhat greater than expected values. For example, nominal 0.20 µm lines are measured as ~0.23 µm, consistent with slight underexposure of the photoresist in these samples. Optimization of development conditions to permit plating at higher doses, coupled with the use of a second generation EUV camera capable of improved image quality, would be expected to give overall improvement in Ni pattern formation and linewidth control in future experiments [37]. Nevertheless, the images in Figures 11A and 11B exhibit good Ni line edge acuity (~10 nm) and vertical sidewalls throughout the entire 0.70 µm planarizer thickness following the RIE. Furthermore, no breakthrough of the thin Ni etch mask is observed for any feature, consistent with uniform deposition and good etch resistance for the Ni films in this application.

A final example of the CCM process used a high-resolution e-beam lithography system as the exposure tool. Figure 12A (next page) shows 100 nm Ni gratings formed using RAY-PN/EDA/Si

after RIE with SF_6-CHF_3 plasma. Variations in Ni linewidths of ~10-15 nm are evident in the grating structures. Examination of this sample following exposure and development (and prior to catalysis and plating) revealed similar variations in feature linewidths, indicative of photoresist

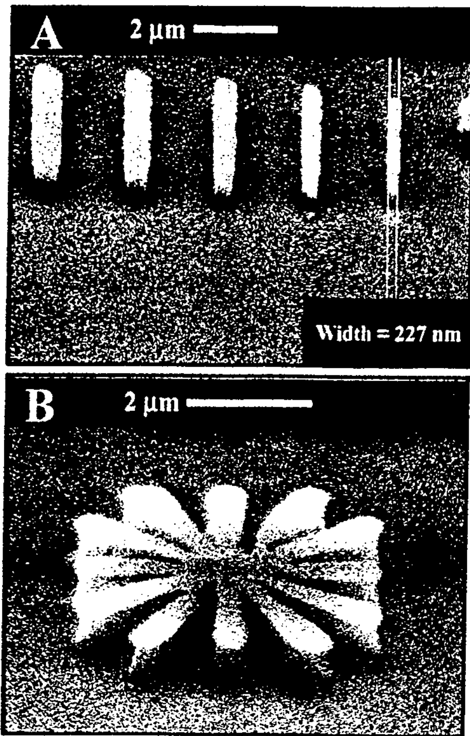

Figure 11. Scanning Electron Micrographs of EUV Patterned Ni Structures on Planarizer After RIE. (A) Isolated Ni lines (light, raised structures) of nominal sizes (left to right) 0.60 µm to 0.20 µm in 0.10 µm steps, and (B) Ni metal star pattern from SAL-601-ER7/EDA/Crosslinked S1400 Planarizer/Si. Process sequence: EUV/Schwartzchild camera (13.4 nm, 8 mJ/cm^2)/PEB (115°C, 2 min)/MF-312 (0.24 M, 6 min)/**PD2** (2 min) 10% NIPOSIT[R] 468 EL Ni (5 min, 25°C)/RIE (O_2 plasma, note Experimental).

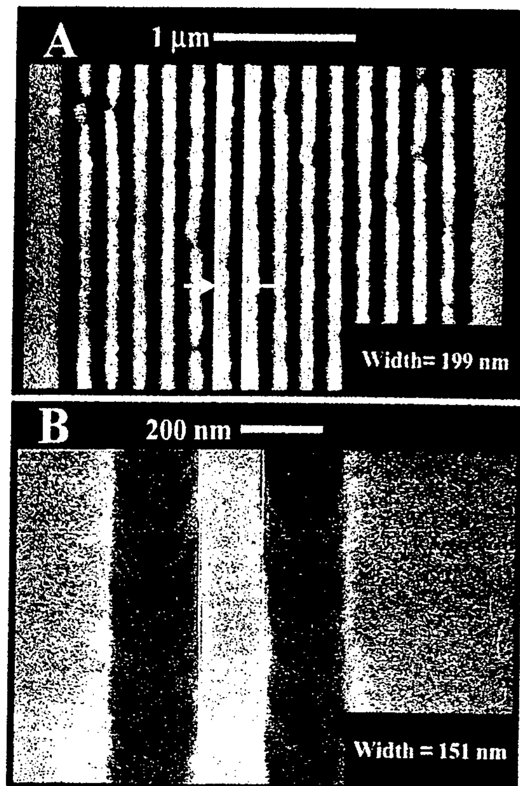

Figure 12. Scanning Electron Micrographs of Electron Beam Patterned Ni Structures on Si After RIE. (A) Equal line/space 0.10 µm Ni (light areas) gratings in RAY-PN EDA/Si. Process sequence: JEOL e-beam nanowriter (50 keV, 20 µC/cm^2) PEB (100°C, 2 min)/MF-312 (0.27 M, 30 sec)/**PD2** (2 min)/10% NIPOSIT[R] 468 EL Ni (5 min, 25°C)/ /XP91140 photoresist remover (80°C, 10 sec)/RIE (SF_6/CHF_3, note Experimental); (B) 0.15 µm Ni line (light area) in SAL-601-ER2/EDA/Si. Process sequence: JEOL e-beam nanowriter (50 keV, 15 µC/cm^2)/ PEB (115°C, 1 min) MF-312 (0.27 M, 90 sec)/**PD2** (2 min)/10% NIPOSIT[R] 468 EL Ni (8 min, 25°C)/XP91140 photoresist remover (80°C, 10 sec) RIE (SF_6-CHF_3 plasma, note Experimental).

proximity effect contributions to linewidth variability in this system. Variations in Ni film thickness, as evidenced by gradations in the Ni line intensity, are also observed. The origin of such mask thickness variations is unknown; it may simply reflect Ni overgrowth of sporadic photoresist residues

in the developed channels, leading to somewhat thinner metal in such areas.[6] Regardless of the origin, however, a Ni mask of sufficient thickness to withstand RIE during pattern transfer ~0.5 μm into the Si substrate is successfully fabricated using the CCM process.

Superior results were obtained through substitution of SAL-601-ER2 for the RAY-PN photoresist. Figure 12B shows a 0.15 μm Ni line formed through e-beam exposure of SAL-601-ER2/EDA/Si after transfer of the pattern ~0.5 μm into the Si substrate using the SF_6-CHF_3 RIE. The variation in intensity across the Ni line is minimal in this case, consistent with the presence of a more uniform mask thickness in this sample compared to Figure 12A. Furthermore, the nominal 0.15 μm Ni line is measured as 0.15 μm with an edge acuity of ~5-10 nm, indicative of good feature CD control in the system. Consequently, through judicious choice of photoresist and SA film coupled with proper control of exposure and development conditions, fabrication of sufficiently robust metal etchmasks for RIE pattern transfer can be realized for feature resolutions to ~0.1 μm using an e-beam based CCM process.

4. Summary and Conclusions

We have described a novel bilevel channel-constrained metallization process combining photoresist patterning and selective EL metal deposition on ligand SA film surfaces for the fabrication of high resolution metal structures useful as etchmasks and conductive interconnects for electronics applications. The technique possesses many desirable attributes and satisfies a number of the conditions required for a manufactureable lithographic process. A particularly attractive advantage of the method is the ability to partition the imaging and pattern transfer functions normally performed by the photoresist in single level lithographic processes between the photoresist and metal films, respectively, in the CCM process. The additional degree of freedom afforded under these circumstances allows the performances of the imaging polymer film and plasma etch resistant metal masking layer to be separately optimized. For example, because the photoresist need not function as an etchmask, film thickness can be adjusted to compensate for DOF and transparency limitations associated with the use of high energy exposure sources.[1] In this manner, the process has been successfully implemented for metal pattern fabrication using optical (*e.g.*, i-line [23], DUV(contact printing 220-230 nm [23], stepper 248 nm), EUV(13.4 nm)) and e-beam sources [55]; pattern formation using nominal photoresist doses at resolutions corresponding to the limits of each exposure tool have been demonstrated.

The choice of metal films as plasma etch resistant masking layers confers additional process advantages. Plating initiates on a ligand SA film that provides a uniform chemical environment, regardless of the underlying substrate, for adherent metal deposition. Metal growth occurs additively and selectively within the photoresist channels; the channel walls maintain control of feature edge acuity while restraining the lateral metal growth associated with loss of feature CD control. Because defects are healed during the growth process and the metal exhibits high plasma etch resistance, thin metal films (required as photoresist thicknesses are adjusted to maintain DOF and transparency during high energy exposures) can function as efficient etchmasks. Furthermore, the EL metal deposition process is aqueous based and requires no complex equipment to implement. Consequently, it provides a cost-effective, track-compatible means for deposition of a metal etchmask in a manufacturing environment.

Despite these advantages, however, two major challenges remain before the CCM process can be seriously considered as a viable manufacturing technology. These comprise issues of photoresist residue clearance and catalyst reagent stability. Physical blockage of surface ligand binding sites by photoresist scums has been demonstrated as a major cause of failure to replicate mask features in metal on the substrate. Plating failure occurs because the residues disrupt the covalent binding interactions between the colloidal Pd(II) particles and the ligand SA film required to anchor the particle to the surface. In a conventional lithography process, the exposed and developed photoresist pattern might be subjected to a light O_2 plasma etch, or de-scum, to remove the residues from the cleared fields. This is not feasible with the CCM process as such a plasma treatment would destroy the ligand functionality of the SA film required for catalyst binding. Consequently, practical residue removal strategies are restricted to those involving more aggressive development to remove the scum from the channels in conjunction with altered exposure doses to compensate for the accompanying linewidth variations. However, because the photoresist adhesion also varies with the nature of the SA film, more aggressive development may also promote photoresist lift-off and subsequent overmetallization for higher resolution features. Such factors collectively lead to overall process latitudes that are narrower than those required for manufactureable processes.

The challenges of attaining long-term (*i.e.*, > 3 months) catalyst reagent stability have been discussed in detail elsewhere [27, 30]. Briefly, the issue involves competition for the labile coordination sites at the Pd(II) centers comprising the colloidal catalyst particles. Labile Cl^- and H_2O species coordinated to the Pd(II) sites can be displaced by surface ligands to covalently bind the particle to the SA film or they can function as bridging ligands to bind one particle to another. In the latter case, particle size slowly and continuously increases as the agglomeration process progresses; the colloids are eventually destabilized and settling of the dispersion occurs. Attempts to chemically modify the particle to prevent the particle bridging reaction will also hinder the surface binding reaction and are therefore not feasible.

Fortunately, the technical difficulties associated with the process do not appear to represent insurmountable problems. They originate, at least in part, from our use of "off-the-shelf" reagents in the practice of the CCM process. For example, both the **PD1** and **PD2** catalysts were originally developed for use with directly patterned SA films [16, 38], where properties such as reproducibility and particle size, rather than long-term stability, were emphasized. Although such materials function as effective proxies for process development, other catalysts may prove superior. Metal colloid catalysts, such as those of Au(0) [56] or Pd(0) [32, 54], comprise potentially attractive alternatives to the Pd(II) colloids constituting **PD1** and **PD2**. Metal colloid dispersions are stable for extended periods and can be covalently bound by strong π-acceptor ligands such as those containing P or S [32]. In addition, because of their net negative surface charge, electrostatic binding of metal colloids at cationic surface sites can also occur. In fact, we have recently exploited the latter binding mode to directly pattern Au(0) metal colloids on protonated EDA SA films [54]. The bound Au retained its ability to initiate EL Ni deposition; deposited Ni films were sufficiently homogeneous and adherent to function as efficient etchmasks for pattern transfer into a Si substrate.

Commercial photoresists are likewise designed for use in conventional (*i.e.*, single level) lithographic processes, where residues do not impact process reliability to the same extent observed in the bilevel CCM process. Alternative photoresist formulations have been developed that yield scum-free channels following exposure and development. For example, post-development residues in

positive tone photoresists can be eliminated through careful control of the degree and pattern of DNQ substitution on the PAC [57] or the molecular weight distribution of the novolak polymer [58] without significant change in lithographic performance. Use of such formulations as imaging layers would be expected to increase process latitude and, consequently, enhance the lithographic performance of the CCM process.

We note in closing that the utility of patterned reactivity templates created via the CCM process extends beyond simple metallization. In fact, fabrication of metal etchmasks for IC applications constitutes a most severe test of the process, given the nature of the plating chemistry and the stringent requirements associated with CD control and edge acuity for high resolution features. Patterns of conducting polymers [59] for liquid crystal display research, poly(dimethylsiloxane) flow channels [60, 61] for cell vascularization studies, and DNA [62] for biosensor/assay applications have already been demonstrated using appropriately modified versions of the process described here. Patterning is often facilitated in these cases because of the less stringent feature resolution requirements and generally simpler attachment chemistries associated with these applications. As our experience with the channel constrained approach increases and further process improvements are made, additional applications in these and related fields can certainly be expected.

5. Acknowledgements

The financial support of Shipley Co. and the Office of Naval Research for this work is gratefully acknowledged. We also thank C. Dulcey for XPS and Auger analyses, R. Gossett and C. Cotell for RBS analyses, and C. Marrian for helpful discussions concerning e-beam lithography and etching. The authors are also grateful to J. Kosakowski, K. W. Rhee and L. M. Shirey of NRL for assistance with the plasma etching experiments and J.M. Calvert and G.N. Taylor of Shipley Company for helpful discussions and use of the laser stepper. The authors thank AT&T for use of the Helicon plasma etcher and G. Kubiak and Sandia National Laboratory for the EUV exposures.

6. References

[1] See, *e.g.*, *Metallized Plastics 2: Fundamental and Applied Aspects*, K.L. Mittal, Editor, Plenum Press, New York (1991), and references therein.

[2] O. Nalamasu, F.A. Baiocchi and G.N. Taylor, in *Polymers in Microlithography*, E. Reichmanis, S.A. MacDonald and T. Iwayanagi, Editors, ACS Symposium Series No. 412, p. 189, American Chemical Society Press, Washington, DC (1989).

[3] R.A. Srinivas, A. Rosen, and A. Heller, *J. Electrochem. Soc.*, **140**, 3021 (1993).

[4] M.L. Schilling, H.E. Katz, F.M. Houlihan, J.M. Kometani, S.M. Stein, and O. Nalamasu, *Proc. SPIE*, **2195**, 182 (1994).

[5] J.M. Calvert, C.S. Dulcey, J.H. Georger, M.C. Peckerar, J.M. Schnur, P.E. Schoen, G.S. Calabrese, and P. Sricharoenchaikit, *Solid State Technology*, **34(10)**, 77 (1991).

[6] G.O. Mallory and J.B. Hadju, *Electroless Plating: Fundamentals and Applications*, American Electroplaters and Surface Finishing Society Press, Orlando, FL (1990).

[7] W. Ehrfeld, P. Bley, F. Gotz, P. Hagmann, A. Maner, J. Mohr, H.O. Moser, D. Muchmeyer, W. Schelb, D. Schmidt, and E.W. Becker, *Proc. IEEE*, **11/1-1**, 160 (1987).

[8] J.S.H. Cho, H.K. Kang, S.S. Wong, and Y. Shacham-Diamond, *Bull. Mat. Res. Soc.*, June 1993, p. 31.

[9] W.J. Dressick, C.S. Dulcey, J.H. Georger, and J.M. Calvert, *Chem. Mater.*, **5**, 148 (1993).

[10] J.M. Calvert, W.J. Dressick, C.S. Dulcey, J.H. Georger, D.A. Stenger, T.S. Koloski, and G.S. Calabrese, in *Polymers for Microelectronics*, American Chemical Society Symposium Series; C.G. Willson, L.F. Thompson, and S. Tagawa, Editors, Vol. 537, p. 210, American Chemical Society Press, Washington, DC (1993).

[11] W.J. Dressick, C.S. Dulcey, J.H. Georger, G.S. Calabrese, and J.M. Calvert, *J. Electrochem. Soc.*, **141**, 210 (1994).

[12] T.S. Koloski, C.S. Dulcey, Q.J. Haralson, and J.M. Calvert, *Langmuir*, **10**, 3122 (1994).

[13] B. Arkles, in *1992 Hüls Silicon Compounds Register and Review*; Anderson, R.; Larson, G.L.; Smith C., Editors, p. 59, Hüls America Inc., Piscataway, NJ (1992).

[14] E.P. Pleuddeman, *Silane Coupling Agents*, Plenum Press, New York (1982).

[15] J.M. Calvert, *J. Vac. Sci. Tech. B*, **11(6)**, 2155 (1993).

[16] W.J. Dressick and J.M. Calvert, *Jap. J. Appl. Phys.*, **32**, 5829 (1994).

[17] T.G. Vargo, J.A. Gardella, J.M. Calvert, and M.S. Chen, *Science*, **262**, 1711 (1993).

[18] J.M. Calvert, P.E. Pehrsson, C.S. Dulcey, and M.C. Peckerar, *Proc. Mater. Res. Soc.*, **260**, 905 (1992).

[19] J.M. Calvert, T.S. Koloski, C.S. Dulcey, W.J. Dressick, M.C. Peckerar, F. Cerrina, J. Taylor, D. Suh, O. Wood, A.A. MacDowell, and R. D'Sousza, *Opt. Eng.*, **32(10)** 2437 (1993).

[20] C.S. Dulcey, T.S. Koloski, W.J. Dressick, M.S. Chen, and J.M. Calvert, *Proc. SPIE*, **1925**, 657 (1993).

[21] C.R.K. Marrian, F.K. Perkins, S.L. Brandow, T.S. Koloski, E.A. Dobisz, and J.M. Calvert, *Appl. Phys. Let.*, **64(3)**, 390 (1994).

[22] F.K. Perkins, E.A. Dobisz, S.L. Brandow, T.S. Koloski, J.M. Calvert, K.W. Rhee, J.E. Kosakowski, and C.R.K. Marrian, *J. Vac. Sci. Tech. B*, **12(6)**, 3725 (1994).

[23] J.M. Calvert, G.S. Calabrese, J.F. Bohland, M-S. Chen, W.J. Dressick, C.S. Dulcey, J.H. Georger, Jr., J. Kosakowski, E.K. Pavelcheck, K.W. Rhee, and L.M. Shirey, *J. Vac. Sci. Tech. B*, **12(6)**, 3884 (1994).

[24] D. Kleinfeld, K.H. Kahler, and P.E. Hockberger, *J. Neurosci.*, **8(11)**, 4098 (1988).

[25] A related process in which a Pd solution reacts directly with the substrate to produce a catalytic seed layer, and EL metal deposition proceeds in constrained structures such as via holes is described in: C.H. Ting and M. Paunovic, *J. Electrochem. Soc.*, **136**, 456 (1989).

[26] R.E. Geer, D.A. Stenger, M.S. Chen, J.M. Calvert, R. Shashidhar, Y.H. Jeong, and P.S. Pershan, *Langmuir*, **10**, 1171 (1994).

[27] S.L. Brandow, W.J. Dressick, C.R.K. Marrian, G-M. Chow, and J.M. Calvert, *J. Electrochem. Soc.*, **142**, 2233 (1995).

[28] C.S. Dulcey, J.H. Georger, Jr., M-S. Chen, S.W. McElvaney, C.E. O'Ferrall, V.I. Benezra, and J.M. Calvert, *Langmuir*, **12**, 1638 (1996).

[29] W.J. Dressick, L.M. Kondracki, M-S. Chen, S.L. Brandow, E. Matijević, and J.M. Calvert, *Coll. Surf. A*, **108**, 101 (1996).

[30] S.L. Brandow, M-S. Chen, T. Wang, C.S. Dulcey, J.M. Calvert, J.F. Bohland, G.S. Calabrese, and W.J. Dressick, *J. Electrochem. Soc.*, **144**, 3425 (1997).

[31] M.L. Schilling, H.E. Katz, F.M. Houlihan, S.M. Stein, R.S. Hutton, and G.N. Taylor, *J. Electrochem. Soc.*, **143**, 691 (1996).

[32] P.M. Maitlis, *The Organic Chemistry of Palladium: Metal Complexes*, Vol. 1, Academic Press, New York (1971), and references therein.

[33] See, *e.g.*, S.P. Murarka and M. Peckerar, *Electronic Materials Science & Technology*, Academic

Press, New York (1989). and references therein.
[34] S. Das, J. Thackeray, M. Endo, J. Langston, and H. Gaw, *Proc. SPIE*, **1262**, 60 (1990).
[35] D.A. Stenger, J.H. Georger, C.S. Dulcey, J.J. Hickman, A.S. Rudolph, T.B. Nielsen, S.M. McCort, and J.M. Calvert. *J. Am. Chem. Soc.*, **114**, 8435 (1992).
[36] W. Moreau, *Semiconductor Lithography*, Ch. 8, Plenum Press, New York (1988).
[37] G. Kubiak, personal communication.
[38] W.J. Dressick, C.S. Dulcey, M-S. Chen, and J.M. Calvert, *Thin Solid Films*, **284-285**, 568 (1996).
[39] A.M.T. van der Putten and J-W. G. deBakker, *J. Electrochem. Soc.*, **140**, 2229 (1993).
[40] A.M.T. van der Putten and J-W. G. deBakker, *J. Electrochem. Soc.*, **140**, 2221 (1993).
[41] S. Asaumi and M. Furuta. *J. Electrochem. Soc.*, **139**, 889 (1992).
[42] S. Asaumi and H. Nakane. *J. Electrochem. Soc.*, **137**, 2546 (1990).
[43] M. Olim, *J. Electrochem. Soc.*, **144**, 4331 (1997).
[44] T. Smy, L.Tan, S.K. Dew, M.J. Brett, Y. Shacham-Diamond, and M. Desilva, *J. Electrochem. Soc.*, **144**, 2215 (1997).
[45] S. Ojima, T. Jizaimaru, S. Omae, and T. Ohmi, *J. Electrochem. Soc.*, **144**, 4005 (1997).
[46] J.N. Hebert and N. Saha, *J. Adhesion Sci. Tech.*, **5(10)**, 905 (1991).
[47] J.J. Ponjeé, V.B. Marriott. M.C.B.A. Michielson, F.J. Touwslager, P.N.T. van Velzen, and H. van der Wel, *J. Vac. Sci. Tech. B*, **8(3)**, 463 (1990).
[48] D.V. Vezenov, A. Noy, L.F. Rosznyai, and C.M. Lieber, *J. Am. Chem. Soc.*, **119**, 2006 (1997).
[49] A. Noy, C.D. Frisbie, L.F. Rosznyai, M.S. Wrighton, and C.M. Lieber, *J. Am. Chem. Soc.*, **117**, 7943 (1995).
[50] J.E. Hudson and H.D. Abruña, *J. Am. Chem. Soc.*, **118**, 6303 (1996).
[51] R.C. Thomas, J.E. Houston, R.M. Crooks, T. Kim, and T.A. Michalske, *J. Am. Chem. Soc.*, **117**, 3830 (1995).
[52] C.W. Jurgensen, A.E. Novembre, and E.S.G. Shaqfeh. *Proc. SPIE*, **1262**, 94 (1990).
[53] S.L. Brandow, J.M. Calvert, E.S. Snow, and P.M. Campbell, *J. Vac. Sci. Tech. B*, **15(3)**, 1455 (1997).
[54] S.L. Brandow, W.J. Dressick, C.S. Dulcey, T.S. Koloski, L.M. Shirey, J. Schmidt, and J.M. Calvert, *J. Vac. Sci. Tech. B*, **15(5)**, 1 (1997).
[55] G.S. Calabrese, J.M. Calvert, W.J. Dressick, C.S. Dulcey, J.H. Georger, Jr., J.F. Bohland, Jr., *U.S. Patent 5,510,216* (1996).
[56] H.B. Weiser, *Inorganic Colloid Chemistry: Volume I- The Colloidal Elements*, Ch. 3, John Wiley & Sons, New York (1933).
[57] R. Hanawa, Y. Uetani, M. Hanabata, *Proc. SPIE*, **1925**, 227 (1993).
[58] A. Zampini, P. Turci, G.J. Cernigliaro, H.F. Sandford, G.J. Swanson, C.C. Meister and R. Sinta, *Proc. SPIE*, **1262**, 501 (1990).
[59] L.Huang, C. O'Ferrall, T.Vargo, R. Shashidhar, W. Fritz, S. Smith, R. Hewitt, and W. Doane, *Proc. SPIE*, **3015**, 150 (1997).
[60] M.A. Bucaro, J.M. Calvert, A.S. Rudolph, B. Spargo, and R. Kapur, *Proc. 16th Southern Biomedical Engineer. Conf. IEEE*, **ISBN 0-7803-3869-3**, 217 (1997).
[61] R. Kapur, B.J. Spargo, M-S. Chen, J.M. Calvert, and A.S. Rudolph, *J. Biomedical Maters. Res. (Appl. Biomaters.)*, **33**, 205 (1996).
[62] L.A. Chrisey, C.E. O'Ferrall, B.J. Spargo, C.S. Dulcey, and J.M. Calvert. *Nucl. Acids Res.*, **24(15)**, 3040 (1996).